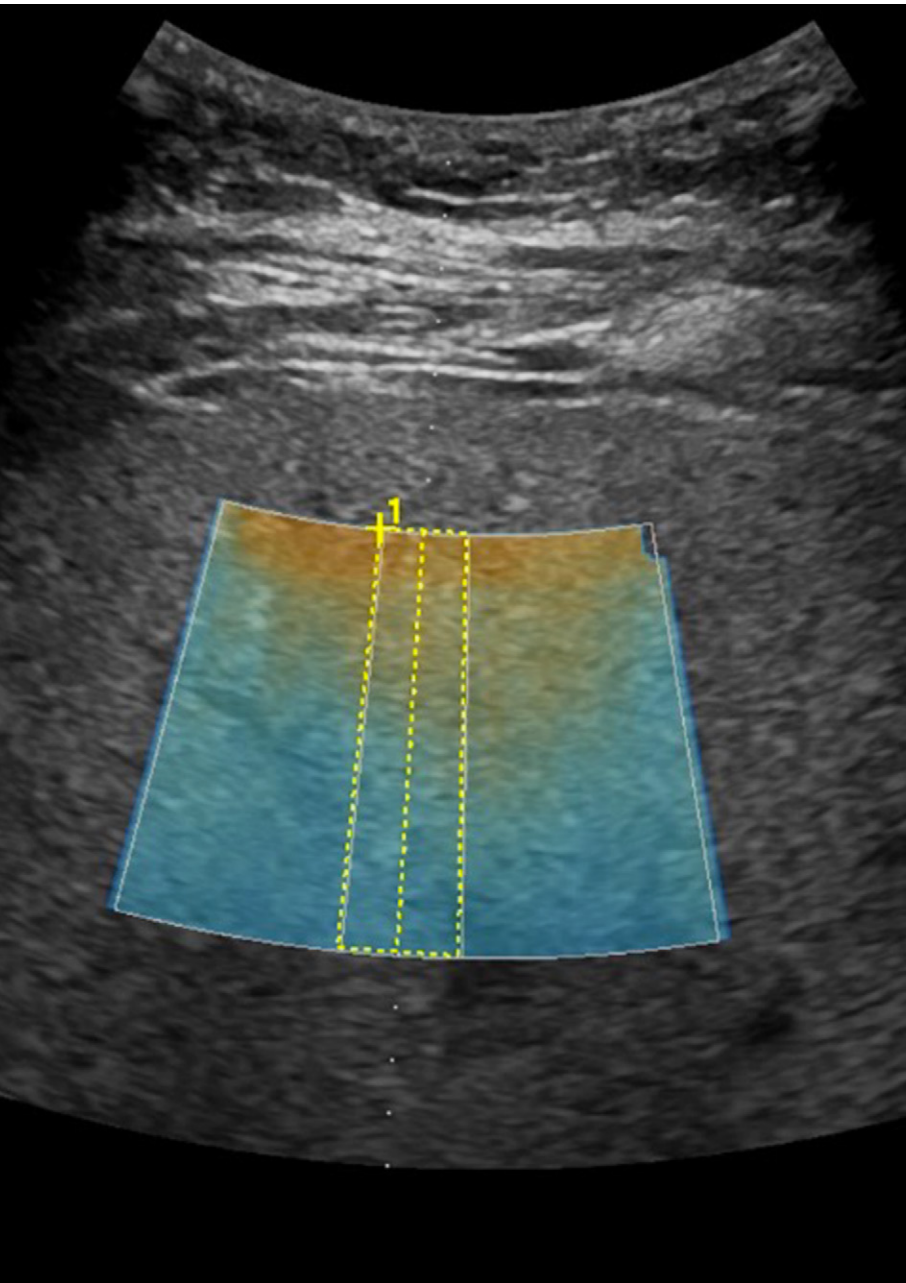


# US Quantification of Liver Fat: Past, Present, and Future

David T. Fetzer, MD • Theodore T. Pierce, MD, MPH • Michelle L. Robbin, MD, MS • Guy Cloutier, PEng, PhD • Arjmand Mufti, MD  
Timothy J. Hall, PhD • Anil Chauhan, MD • Reinhard Kubale, MD • An Tang, MD, MSc, FRCPC

Author affiliations, funding, and conflicts of interest are listed at [the end of this article](#).



Fatty liver disease has a high and increasing prevalence worldwide, is associated with adverse cardiovascular events and higher long-term medical costs, and may lead to liver-related morbidity and mortality. There is an urgent need for accurate, reproducible, accessible, and noninvasive techniques appropriate for detecting and quantifying liver fat in the general population and for monitoring treatment response in at-risk patients. CT may play a potential role in opportunistic screening, and MRI proton-density fat fraction provides high accuracy for liver fat quantification; however, these imaging modalities may not be suited for widespread screening and surveillance, given the high global prevalence. US, a safe and widely available modality, is well positioned as a screening and surveillance tool. Although well-established qualitative signs of liver fat perform well in moderate and severe steatosis, these signs are less reliable for grading mild steatosis and are likely unreliable for detecting subtle changes over time. New and emerging quantitative biomarkers of liver fat, such as those based on standardized measurements of attenuation, backscatter, and speed of sound, hold promise. Evolving techniques such as multiparametric modeling, radiofrequency envelope analysis, and artificial intelligence-based tools are also on the horizon. The authors discuss the societal impact of fatty liver disease, summarize the current state of liver fat quantification with CT and MRI, and describe past, currently available, and potential future US-based techniques for evaluating liver fat. For each US-based technique, they describe the concept, measurement method, advantages, and limitations.

©RSNA, 2023 • [radiographics.rsna.org](http://radiographics.rsna.org)

## Supplemental Material



Quiz questions for this article are available through the [Online Learning Center](#).

RadioGraphics 2023; 43(7):e220178  
<https://doi.org/10.1148/rq.220178>

Content Codes: GI, US

**Abbreviations:** AUROC = area under the receiver operating characteristic curve, CAP = controlled attenuation parameter, I/Q = in-phase and quadrature demodulated, NAFLD = nonalcoholic fatty liver disease, NASH = nonalcoholic steatohepatitis, PACS = picture archiving and communication system, PDFF = proton-density fat fraction, ROI = region of interest, SoS = speed of sound, SWD = shear wave dispersion, SWS = shear wave elastography, UDFP = US-derived fat fraction, VCTE = vibration-controlled transient elastography

### TEACHING POINTS

- The hepatorenal index is a US technique for indirectly and semiquantitatively measuring steatosis as the echogenicity ratio of the liver to right kidney cortex.
- The attenuation coefficient is the measurement of acoustic energy loss as an acoustic wave propagates through a medium, typically at a specific frequency.
- The backscatter coefficient refers to measurement of ultrasound echoes attributed to reflection and scattering, data that are the primary determinant of gray-scale brightness in B-mode imaging.
- SoS is the longitudinal compression (acoustic) wave propagation velocity in a medium, which varies depending on material composition—for example, 1450 m/sec in fat and 1550 m/sec in liver.
- Combination of several quantitative parameters into a composite technique may correct for sources of variability and improve correlation with liver fat content. One such method—modeling phantom-corrected attenuation and backscatter—has shown promise, now commercially available as US-derived fat fraction (UDFF).

### Introduction

Hepatic steatosis, also known as fatty liver, is a common imaging finding with important medical and societal implications. Steatosis is defined as the presence of excessive lipid within 5% of hepatocytes or more and may be the result of viral hepatitis, excessive alcohol consumption, certain medications or chemotherapy agents, or intestinal malabsorption (1). Nonalcoholic fatty liver disease (NAFLD) is the presence of steatosis in the absence of these secondary causes and is considered the hepatic manifestation of metabolic syndrome, associated with obesity, type II diabetes, dyslipidemia, and hypertension (1). The spectrum of NAFLD ranges from simple steatosis to nonalcoholic steatohepatitis (NASH), the latter characterized histologically by the presence of lobular inflammation, hepatocyte ballooning, and fibrosis (2).

NAFLD and NASH represent a large and growing public health concern. NAFLD is now the leading cause of chronic liver disease worldwide, affecting 25%–30% of the global population and accounting for approximately 75% of chronic liver disease in the United States (3,4). NASH is modeled to increase by up to 56% in western Europe, China, and the United States by 2030 (5).

Patients with NAFLD have increased overall mortality from hepatic and nonhepatic causes (6). Cardiovascular disease is the most common cause of death in this population, with cancer and liver-related mortality making up the additional leading causes (7). Patients with NASH may develop

advanced fibrosis or cirrhosis, with development of hepatocellular carcinoma at similar rates as in patients with alcoholic cirrhosis (~10–15 per 1000 person-years) (8). NAFLD is now the fastest-growing cause of hepatocellular carcinoma in the world and the underlying disease in 14% of cases of hepatocellular carcinoma in the United States (3,8). NAFLD is also the fastest-growing cause of liver transplant in the United States (9).

Identifying individuals in the general population with hepatic steatosis (screening) is becoming more important, as the long-term health care expenditure for patients with NAFLD is 80% higher than for a non-NAFLD control subject of similar age and metabolic comorbidities (10). Although only a minority of patients with NAFLD also have NASH, up to 30% of patients with NASH may develop advanced fibrosis or cirrhosis (2). Also, some emerging pharmaceutical agents use hepatic steatosis as a biomarker of response to therapy. Therefore, follow-up of patients with NAFLD becomes important (surveillance).

With the high prevalence of steatosis in the general population, liver biopsy is not practical. In addition to the associated costs and risks, liver biopsy is subject to sampling error, and histologic assessment for steatosis is qualitative with considerable interobserver variability, making it less than ideal for diagnosis and longitudinal follow-up (11). Given these shortcomings, there is an urgent need for accurate, reproducible, and noninvasive methods for evaluation of steatosis. Although MRI is accurate for quantifying steatosis and CT may be useful in opportunistic detection, their use in generalized screening and surveillance may be impacted by accessibility limitations, cost, and applicable risks and contraindications.

This review focuses on use of US for assessment of steatosis. Nonimaging techniques and non-US-based imaging techniques are briefly introduced. Then, the impact of steatosis on ultrasound wave propagation and backscatter is reviewed. Finally, traditional, new, and emerging US techniques for detection, grading, and quantification of liver fat are highlighted, including an overview of the concept and the measurement method, advantages, and limitations of each technique.

### Current Nonimaging Techniques

Fatty liver disease may be suspected clinically on the basis of individual patient risk factors and abnormalities in basic liver function test results. Additional serum panels and other nonimaging tests performed in the office may assist in further risk assessment, results of which could trigger confirmatory imaging studies.

### Clinical Markers of Steatosis

Several clinical panels that incorporate various risk factors, anthropomorphic data, and blood tests have been investigated for assessment of hepatic steatosis, including the Fatty Liver Index, Hepatic Steatosis Index, NAFLD Liver Fat Score, SteatoTest, NAFLD Ridge Score, and NAFL Screening Score. Diagnosis of steatosis (>5%) with the NAFLD Liver Fat Score, with the Hepatic Steatosis Index, and with the Fatty Liver Index does not appear to differ substantially, with the area under the receiver operating characteristic curve (AUROC) ranging between 0.80 and 0.83 (12). However, many of these

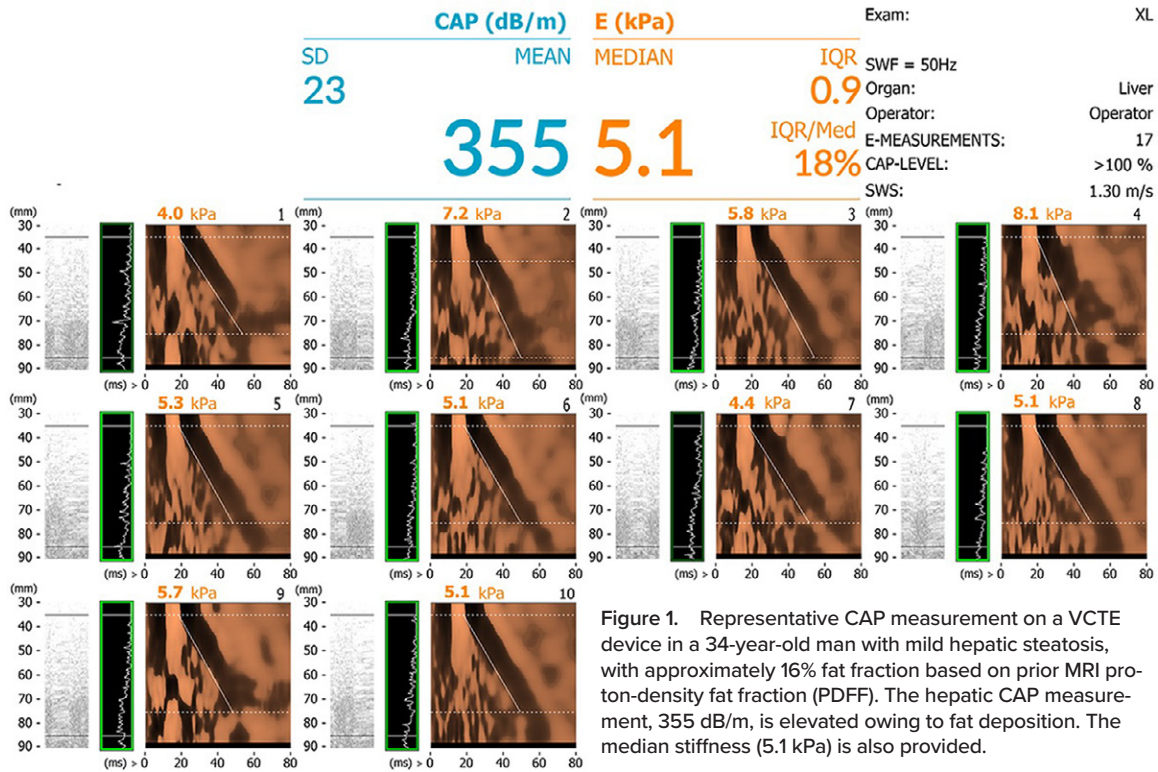


Figure 1. Representative CAP measurement on a VCTE device in a 34-year-old man with mild hepatic steatosis, with approximately 16% fat fraction based on prior MRI proton-density fat fraction (PDFF). The hepatic CAP measurement, 355 dB/m, is elevated owing to fat deposition. The median stiffness (5.1 kPa) is also provided.

tests may not add significantly to routine clinical information and information on standard serum markers.

Several serum biomarkers and biochemical panels have also been investigated for diagnosis of NASH. Markers of inflammation and inflammatory mediators, oxidative stress, apoptosis, and serum adipocytokines have all been evaluated as potential biomarkers. Panels including the NASH ClinLip-Met Score, NASHTest, and NASH Diagnostics Panel show good accuracy for diagnosis of NASH, although none has emerged as the standard of care (13).

### Controlled Attenuation Parameter

**Concept.**—The controlled attenuation parameter (CAP) is a single-vendor proprietary technique available on vibration-controlled transient elastography (VCTE) devices (FibroScan; Echosens), often implemented in the office at the point of care. CAP measures the total attenuation of sound waves (considered an indirect measure of steatosis, as discussed later) (14).

**Measurement Method.**—CAP measurement and VCTE are performed simultaneously. Attenuation is measured at the central frequency of 3.5 MHz, expressed in decibels per meter. Ten valid measurements within the right hepatic lobe are obtained via an intercostal space, with the median reported (Fig 1) (15). Results may be converted to one of four steatosis grades—S0, S1, S2, or S3—using manufacturer-supplied cutoffs.

**Advantages.**—VCTE is relatively low cost, is available in the office setting, and has reported good interobserver agreement (15–17).

**Limitations.**—Two-dimensional B-mode images are not generated; therefore masses, large vessels, and artifacts may be difficult to avoid, and measurements cannot be obtained in the presence of ascites. Proposed cutoffs vary in the published literature, with AUROC ranging from 0.70 to 0.87 for different steatosis grades (16). Specifically in patients with NAFLD, poor accuracy may preclude grading of steatosis (17). CAP may be confounded by superimposed steatohepatitis and fibrosis or by subcutaneous fat, particularly in obesity (17).

### Non-US-based Imaging Techniques

Many imaging modalities offer techniques for detecting or quantifying liver fat (Table S1). An overview of non-US-based techniques is presented in this section, followed by a more detailed discussion of US-based techniques. Previous review articles discuss in detail CT- and MR-based liver fat quantification (18–20).

#### CT Assessment

**Concept.**—CT is based on x-ray attenuation. Increasing hepatic lipid content causes decreased parenchymal attenuation, which is linearly correlated with MRI proton-density fat fraction (PDFF) (19,21).

**Measurement Method.**—X-ray attenuation in CT is displayed in Hounsfield units. As steatosis worsens, measured Hounsfield unit values decrease. Both relative (normalized to spleen) and absolute Hounsfield unit cutoff values have been reported, with noncontrast CT considered more reliable (Fig 2) (19).

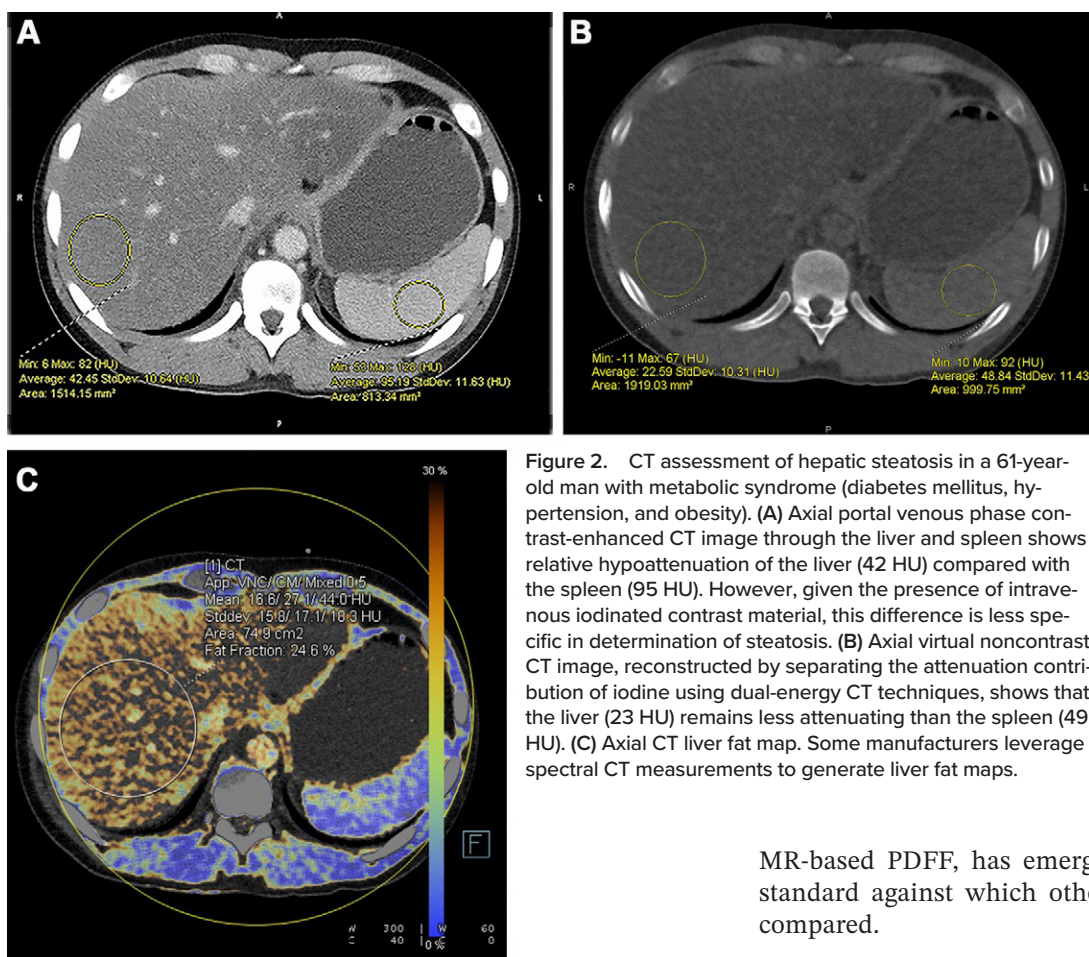


**Figure 2.** CT assessment of hepatic steatosis in a 61-year-old man with metabolic syndrome (diabetes mellitus, hypertension, and obesity). (A) Axial portal venous phase contrast-enhanced CT image through the liver and spleen shows relative hypoattenuation of the liver (42 HU) compared with the spleen (95 HU). However, given the presence of intravenous iodinated contrast material, this difference is less specific in determination of steatosis. (B) Axial virtual noncontrast CT image, reconstructed by separating the attenuation contribution of iodine using dual-energy CT techniques, shows that the liver (23 HU) remains less attenuating than the spleen (49 HU). (C) Axial CT liver fat map. Some manufacturers leverage spectral CT measurements to generate liver fat maps.

**Postprocessing.**—Clinical picture archiving and communication systems (PACS) allow measurement of liver parenchymal Hounsfield unit values by placing a region of interest (ROI) within tissue free of large vessels, masses, and other nonparenchymal structures. With dual-energy CT techniques, material decomposition may separate attenuation contributions from iodine or iron (Fig 2).

**Advantages.**—CT is widely available and reproducible. Non-contrast CT is accurate for detection of moderate liver fat (sensitivity up to 95%, specificity over 90%) (18,21,22). Opportunistic evaluation of steatosis can be performed during CT examinations ordered for other purposes (23).

**Limitations.**—CT provides low sensitivity (57%) for mild steatosis. Given the radiation exposure and relatively high cost, CT is suboptimal for population-level screening or ongoing surveillance. Steatosis assessment may be confounded by intravenous contrast material or hepatocyte iron, copper, or glycogen (19). Parenchymal edema may decrease liver attenuation, mimicking steatosis. Liver attenuation may also be affected by beam-hardening artifact, peak kilovolt potential, or vendor-specific x-ray filters (19).

### MR-based Proton-Density Fat Fraction

MRI has emerged as a sensitive and specific modality for measurement of liver fat (18–20). One specific technique,

MR-based PDFF, has emerged as the surrogate reference standard against which other noninvasive tests are being compared.

**Concept.**—PDFF is calculated as the ratio of MR-visible protons attributable to triglyceride (ie, fat) to the sum of all protons attributable to triglyceride and water (18–20).

**Measurement Method.**—PDFF can be measured with MR spectroscopy or MRI. Briefly, these techniques rely on phase differences in resonance frequency (chemical shift) between water and triglyceride molecules, assessed at multiple echo times. To achieve accurate and unbiased fat quantification, these techniques are corrected for spectral complexity of fat, T1 relaxation effect, and T2 or T2\* relaxation effect (20). MR spectroscopy measures the PDFF from a small volume of liver (typically a voxel of  $25 \times 25 \times 25$  mm), whereas MRI produces a map with pixels matching PDFF values (Fig 3).

**Postprocessing.**—For MRI, ROIs can be drawn on the PDFF maps to estimate the mean fat fraction (as a percentage). Some commercial software provides automated segmentation to compute mean whole-liver PDFF. The following thresholds have been proposed to grade the severity of steatosis: 6.4% to diagnose grade 1 or higher steatosis (mild), 17.4% to diagnose grade 2 or higher steatosis (moderate), and 22.1% to diagnose grade 3 steatosis (severe) (24).

**Advantages.**—MR-PDFF has emerged as an objective assessment of and the most accurate noninvasive biomarker for liver fat, with high accuracy for grading steatosis. PDFF has been studied in large and geographically diverse cohorts and

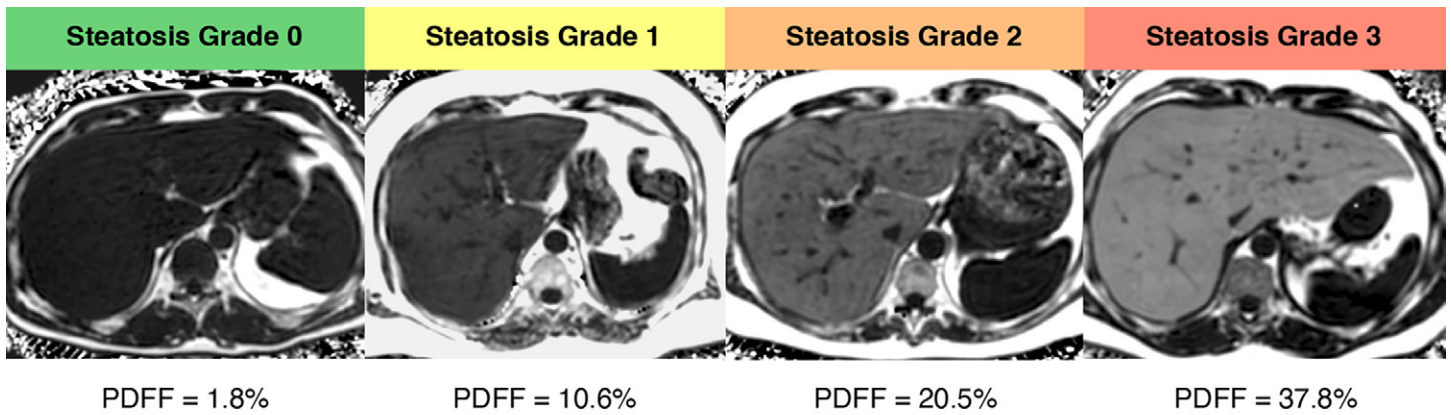


Figure 3. Axial MR-PDFF maps and mean liver PDFF computed from whole-liver segmentation in four patients with biopsy-proven steatosis grades 0–3: 1.8% (grade 0), 10.6% (grade 1), 20.5% (grade 2), and 37.8% (grade 3).

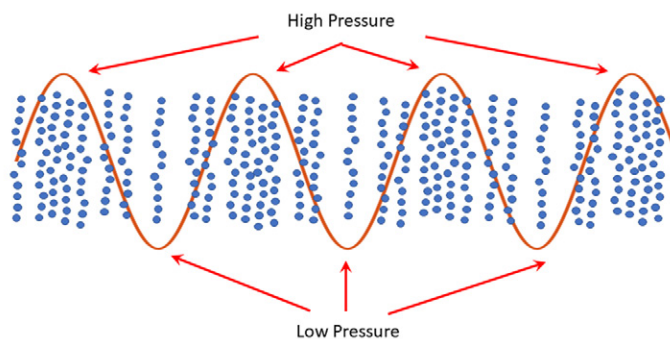


Figure 4. Simplistic simulation of a one-dimensional mechanical (sound) wave shows areas of higher and lower particle density as a result of a passing longitudinal pressure wave, which locally compresses and later expands the particles as a result of locally high and low pressure, respectively (orange sine-wave overlay).

shown to offer high precision using different field strengths, MRI system manufacturers, and reconstruction methods (25). Acquisition time is short, with MRI-PDFF of the entire liver achievable within one breath hold.

**Limitations.**—Widespread deployment of MR-PDFF is affected by cost and availability. While PDFF imaging allows fat quantification, MR spectroscopy is still needed to perform advanced characterization of the type of liver fat, which requires expert postprocessing and analysis.

## US Assessment

### Overview

US is a safe, widely available, and relatively low-cost imaging modality for assessment of liver disease, including evaluation of steatosis (22,26). Liver US is commonly performed in patients with unexplained elevation of liver function test results and to monitor patients with known or suspected chronic liver disease; therefore, US is well positioned to provide an assessment of steatosis for both screening (detection) and surveillance (monitoring). US holds great promise for assessment of steatosis, given the widespread need and lower access barriers.

Liver US is generally performed with a curvilinear (convex) transducer using low transmit frequencies (1–5 MHz). Commonly used qualitative gray-scale image features of steatosis are described later. Newer quantitative techniques are possible, several of which are now commercially available. A description of the interaction between ultrasound and hepatocytes containing fat vacuoles will help in understanding the appearance of liver steatosis on gray-scale or brightness-mode (B-mode) images and the impact on these various quantitative techniques.

### Interaction between Sound and Tissue

**Acoustic Wave Propagation.**—To understand the impact of steatosis (lipid droplets in hepatocytes) on ultrasound, a review of mechanical wave propagation is helpful. Mechanical waves produce physical particle motion. Acoustic (sound) waves, a type of longitudinal mechanical wave, can be considered pressure waves or compression waves because they locally increase (and later decrease) the local pressure of a material through which they are traveling. When these waves propagate through a uniform material, particle motion can be reasonably approximated as a plane wave (one-dimensional) in the direction of travel (Fig 4).

**Sound Speed.**—A material can be described by both its mass density and its compressibility (coefficient of stiffness, or bulk modulus), which influence acoustic wave propagation (27). The speed of sound (SoS) is equal to the square root of stiffness (bulk modulus) divided by density. Therefore, a relatively stiff (noncompressible) tissue will have higher SoS, whereas fat—which is relatively less stiff (more compressible)—will have lower SoS. Compared with water, most soft tissues generally have slightly higher mass density (approximately 1.04 g/cm<sup>3</sup>) and sound speed (1540 m/sec), while lipids generally have lower mass density (0.9 g/cm<sup>3</sup>) and sound speed (approximately 1450 m/sec) (28). So, increasing liver fat is expected to decrease sound speed (Fig 5).

**Backscatter and Speckle.**—When an acoustic wave passes through an inhomogeneous material containing particles of different acoustic impedance (product of a material's mass

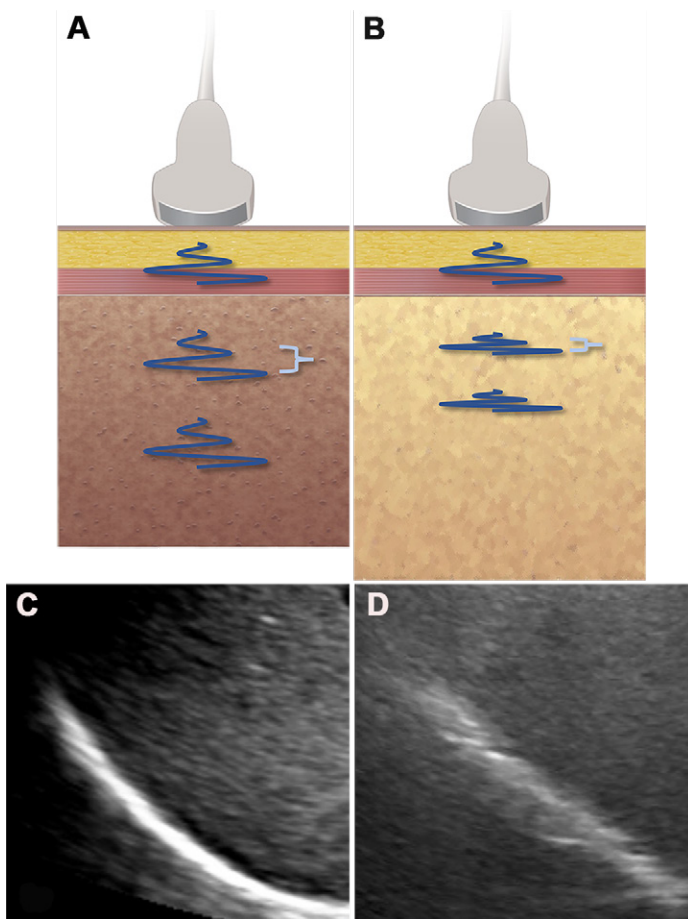


**Figure 5.** Speed of sound (SoS). (A) A material can be characterized by the speed with which an acoustic compression wave propagates through that material. SoS is measured in meters per second. (B) In a steatotic liver, SoS is decreased. As acoustic wave propagation slows, the wavelength shortens as the frequency remains constant (brackets). Not only does this impact beam focusing, but returning echoes arrive later in time than expected, leading to erroneous localization of a structure further from the transducer. (C) In most US applications, beam forming and image generation rely on the assumption of a constant speed of sound, generally 1540 m/sec, which allows precise localization of returning echoes. US image with precise localization of returning echoes shows clear delineation of the diaphragm interface through the right lobe of the liver. (D) In the setting of steatosis, differences in assumed SoS lead to loss of resolution and errors in echo localization. US image in a patient with steatosis shows blurring of the diaphragm. (C and D were obtained with the same device and a convex transducer at 3-MHz central frequency.)

density and sound speed), such as lipid droplets in hepatocytes, some of its energy is absorbed (converted to heat) or redirected (scattered) (29). When the shape of these scatterers is (roughly) spherical, much of that energy is scattered back toward the direction of the incoming wave (backscatter or echo). This backscatter signal is the fundamental principle behind pulse-echo US and generation of B-mode gray-scale images. The magnitude of the backscatter signal (echogenicity) depends on the size, shape, orientation, and acoustic impedance difference between these scatterers and their surroundings. Therefore, an increasing number of lipid droplets is expected to increase backscatter signal (brightness), although wave interferences may reduce backscatter at very high lipid droplet concentration (Fig 6).

When there are several of these scatterers within the acoustic pulse volume, and those scatterers are tiny compared with the wavelength, the resulting backscatter is a summation of acoustic signal from these unresolvable constituents. The constructive and destructive wave interferences from these scatterers contribute to the B-mode parenchymal echotexture (speckle), or the variation in size and brightness of the dots that make up the tissue stroma (30). Larger inhomogeneities (large lipid droplets) may cause the speckle spots to broaden and lengthen.

Another reason why the speckle spots might broaden is ultrasound beam defocusing due to a mismatch between the actual average sound speed in the material and the assumed sound speed assumed by the US system when focusing the transmitted and received ultrasound beam (28). For example, if liver lipid content is 20%, then the average sound speed in the liver is likely reduced from 1540 m/sec to 1522 m/sec (where  $1522 \text{ m/sec} = 0.8 \times 1540 \text{ m/sec} + 0.2 \times 1450 \text{ m/sec}$ ). If the US system uses a sound speed of 1540 m/sec for beam forming, this mismatch leads to poorer focusing of the ultrasound beam and lower image quality (broader speckle spots) (Fig 5).

**Attenuation.**—Attenuation, or the loss of pulse power, results from the combination of absorption, reflection, refraction, scattering, and diffusion of the ultrasound wave as it passes through a material. Qualitative differences in attenuation can be appreciated as enhancement (increased brightness) of tissues deep to a nonattenuating cyst, or as shadowing (decreased brightness) deep to a highly attenuating breast cancer (31). Attenuation is difficult to predict in materials, although liver is one tissue that has been thoroughly studied. Numerous investigations have proposed models to describe the mechanisms contributing to attenuation in liver. Although there is no consensus on the exact influence of these mechanisms on excess attenuation in steatosis compared with normal liver, scattering from lipid droplets (with relatively high acoustic impedance difference compared with surrounding tissue) and absorption are both meaningful (Fig 7).

## Past US Technique

### Assessment of Qualitative Gray-Scale Features

**Concept.**—Steatosis has been evaluated with US since the 1970s. As discussed earlier, steatosis increases average backscatter signal (global parenchymal echogenicity). However, as gray-scale image echogenicity is also reliant on technical factors including transducer frequency, output power, and gain, comparison with internal references is needed. Increasing degrees of steatosis also progressively increase acoustic attenuation, leading to decreased signal from deeper portions of the liver (32). Finally, as steatosis decreases sound speed, increasing image clutter and worsening spatial resolution due to beam-forming and echo-localization errors may be appreciated.

**Measurement Method.**—Diffuse hepatic steatosis is generally categorized at gray-scale US as mild, moderate, or severe,

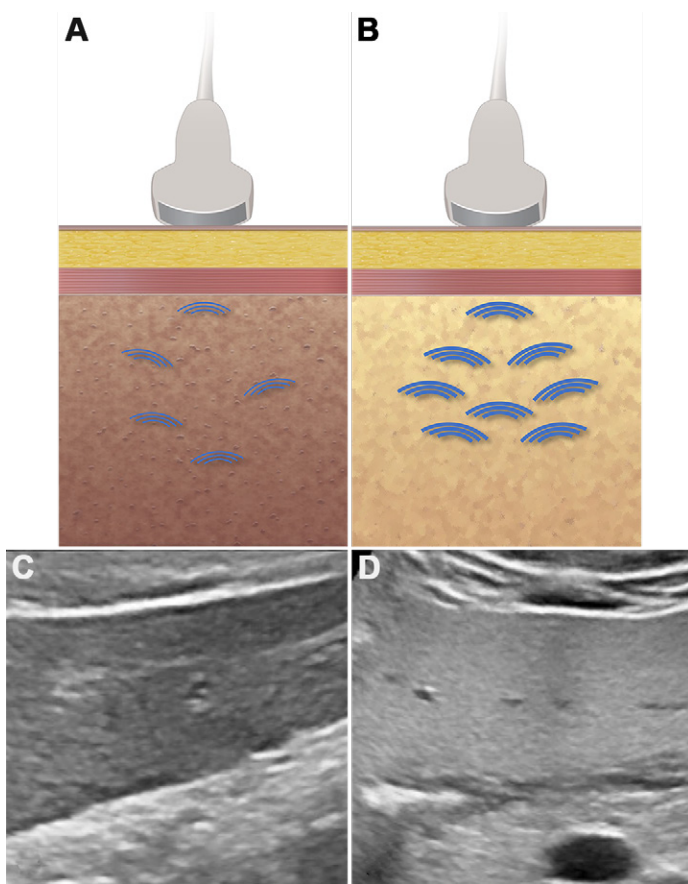


**Figure 6.** Backscatter. (A) Acoustic signal returning to the transducer from unresolvable tissue constituents (backscatter) is the primary determinant of gray-scale brightness in B-mode imaging. The number and strength of this backscatter are influenced by variations in acoustic impedance (density and speed of sound) in small scatterers that compose the tissue stroma (not depicted is the contribution of constructive and destructive wave interferences). (B) When the number of scatterers or the variability in their acoustic impedance increases, backscatter signal is expected to increase. (C, D) US images show this phenomenon between normal liver (C) and steatotic liver (D) as an increase in parenchymal echogenicity (brightness) of the left hepatic lobe. (C and D obtained with the same device and a convex transducer at 3-MHz central frequency.)

based on subjective assessment of several features (22,33) (Figs 8, 9). With increasing steatosis, the echogenicity of the hepatic parenchyma relative to that of the adjacent kidney, pancreas, or spleen increases, while the visibility and clarity of portal vein and gallbladder walls and the diaphragm-lung interface progressively diminish (22,33,34).

Mild steatosis results in a mild increase in liver echogenicity with regard to the adjacent normal right kidney. Moderate steatosis shows a more marked increase in echogenicity and a slight decrease in the conspicuity of vessel borders, the gallbladder wall, and the diaphragm. Severe steatosis shows markedly increased echogenicity, as well as loss of vessel border definition and loss of diaphragm visualization due to decreased ultrasound beam penetration (increased attenuation) (35). Focal fat sparing in the presence of diffuse hepatic steatosis is a specific sign and can be found in typical locations, such as along the gallbladder fossa or the fissure for the falciform ligament or adjacent to the portal vein.

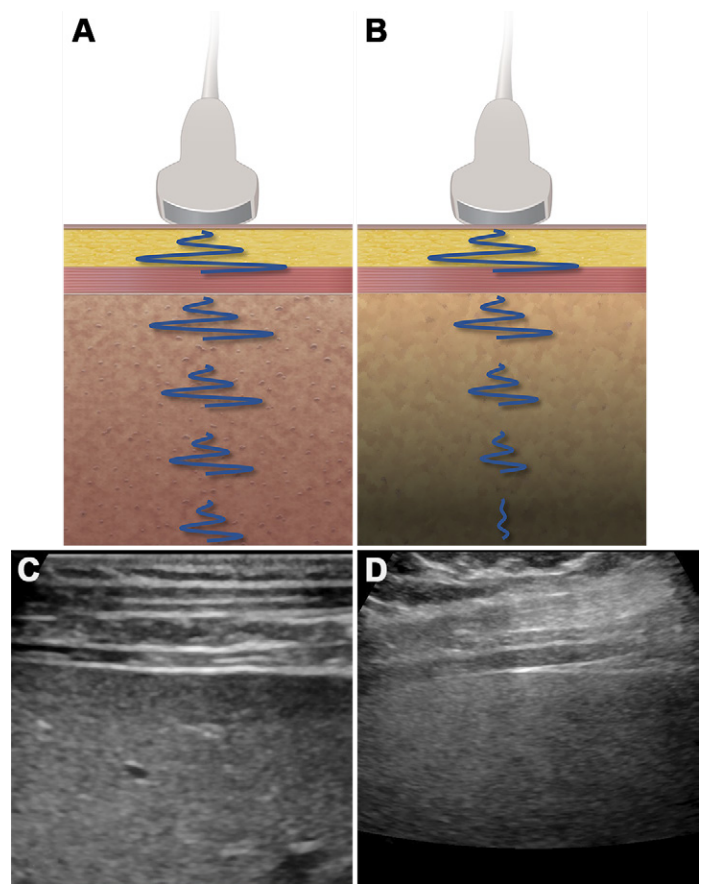


**Figure 7.** Attenuation. (A) As sound pulses travel through a medium, absorption, reflection, refraction, scattering, and diffusion contribute to loss of pulse power. The rate of this power loss is attenuation (expressed in decibels per centimeter at a specific frequency). (B) Increasing liver fat leads to both increased absorption and reflection (backscatter), leading to greater attenuation. (C) US systems assume a constant rate of attenuation to produce a homogeneous gray-scale image. (D) When attenuation is greater than assumed by the system, such as in steatosis, there is progressive darkening of the deeper liver (far field) relative to the more superficial liver (near field). (C and D obtained with the same device and a linear transducer at 7-MHz central frequency.)

**Advantages.**—The subjective assessment can be made on routine gray-scale images; no special postprocessing is needed. A recent meta-analysis calculated a high AUROC of 0.80 for subjective detection of steatosis at US (ie, differentiating intrahepatic fat of  $\geq 5\%$  vs  $< 5\%$ ) (36). Another meta-analysis calculated an AUROC of 0.93 in differentiating moderate to severe hepatic steatosis from no steatosis (37).

**Limitations.**—Body habitus and sonographer experience may limit complete visualization of the liver and acquisition of representative images. Parenchymal appearance can be influenced by the scanning window, shadowing and refraction artifacts, and a large subcutaneous fat layer between the liver and the transducer. Additional technical factors impacting the appearance of the parenchyma include the transducer and frequency, harmonic imaging, gain, and output power. Steatosis evaluation is limited in the setting of fibrosis and other infiltrative diseases and is impacted by renal disease, as an increase in renal echogenicity will decrease apparent hepatic-to-renal contrast (34).

Feature	Normal	Mild	Moderate	Severe
<b>Parenchymal Echogenicity</b>	Hypo- or isoechoic relative to kidney; Hypoechoic relative to pancreas	Progressive increase in echogenicity relative to kidney and pancreas	Markedly echogenic relative to kidney; Isoechoic to pancreas	
<b>Portal Walls; Gallbladder Wall</b>	Echogenic, clearly depicted walls	Progressive decrease in clarity and relative echogenicity of portal and gallbladder walls	Portal and gallbladder walls indistinct	
<b>Attenuation</b>	Uniform appearance of parenchyma from near to far field	Progressive darkening of deeper parenchyma relative to nearfield*	Marked difference in parenchymal visualization, with far field significantly darker and not well visualized	
<b>Clarity of Diaphragm</b>	Clearly depicted, smooth, and highly echogenic	Progressive decrease in clarity and relative echogenicity of diaphragm	Near-complete or complete loss; if visible, may be poorly echogenic and indistinct	
<b>Focal Fat Sparing</b>	None	Conspicuous		

Figure 8. Common B-mode US features in a normal liver and in increasing degrees of steatosis. \* May be overcome with lower transducer frequency and adjustments to time-gain compensation (TGC).

Visual assessment of the various signs of steatosis remains subjective. Detection of mild steatosis, differentiation between steatosis grades, and tracking small changes over time are difficult using conventional techniques (38). Varying sensitivities and cutoffs have been reported, as well as low intrareader and interreader agreement, depending on the criterion analyzed (37,39,40).

### Present US Techniques

#### Semiquantitative Hepatorenal Index

**Concept.**—The hepatorenal index is a US technique for indirectly and semiquantitatively measuring steatosis as the echogenicity ratio of the liver to right kidney cortex. As discussed earlier, increasing liver echogenicity with worsening steatosis is a qualitative feature that generally requires an internal reference.

**Measurement Method.**—To calculate the hepatorenal index, ROIs (suggested diameter ≥ 1 cm) are placed in the liver parenchyma and the right renal cortex on a single image, away from artifacts, masses, and large vessels (Figs 10, 11). Both ROIs should be at the same distance from the transducer to minimize depth-dependent attenuation differences. Various hepatorenal index cutoffs for the presence of steatosis have been published, ranging from 1.24 to 2.2 (31,41–44).

**Advantages.**—The hepatorenal index is a relatively intuitive and reproducible technique for assessment of steatosis (41,42,44). Some manufacturers have implementations for on-scanner calculation. Clinical PACS may permit hepatorenal index estimation, allowing seamless implementation into routine practice, without the need for separate equipment or other additional costs.

**Limitations.**—It has been recommended that individual sites validate cutoffs on the basis of local data and that patients returning for follow-up examinations be imaged on the same device to minimize intermanufacturer variability; however, these recommendations may be impractical for most sites. Some operator and technique dependency remains (Fig 12), widely accepted cutoff values are not yet available, and there is limited literature on intervender variability. Not all PACS can produce hepatorenal indexes, in which case on-scanner calculation can be pursued.

The hepatorenal index assumes a normal kidney (absence of renal disease that may increase cortical echogenicity), and sufficient cortical thickness is needed for ROI placement without including scar or medullary pyramids. Other diffuse liver diseases may increase or decrease relative liver echogenicity, thereby confounding hepatorenal index interpretation.

#### Quantitative Pulse-Echo Techniques

Quantitative pulse-echo techniques include measurement of the attenuation coefficient, backscatter coefficient, and SoS, as well as composite quantitative techniques.

##### Attenuation Coefficient

**Concept.**—The attenuation coefficient is the measurement of acoustic energy loss as an acoustic wave propagates through a medium, typically at a specific frequency (27). Although the effects of attenuation may be difficult to appreciate in diffuse liver disease, particularly when mild, there is a long history demonstrating the correlation between steatosis and attenuation (Fig 7) (31).

**Measurement Method.**—A large ROI is placed in the hepatic parenchyma, avoiding artifacts, masses, and large vessels,

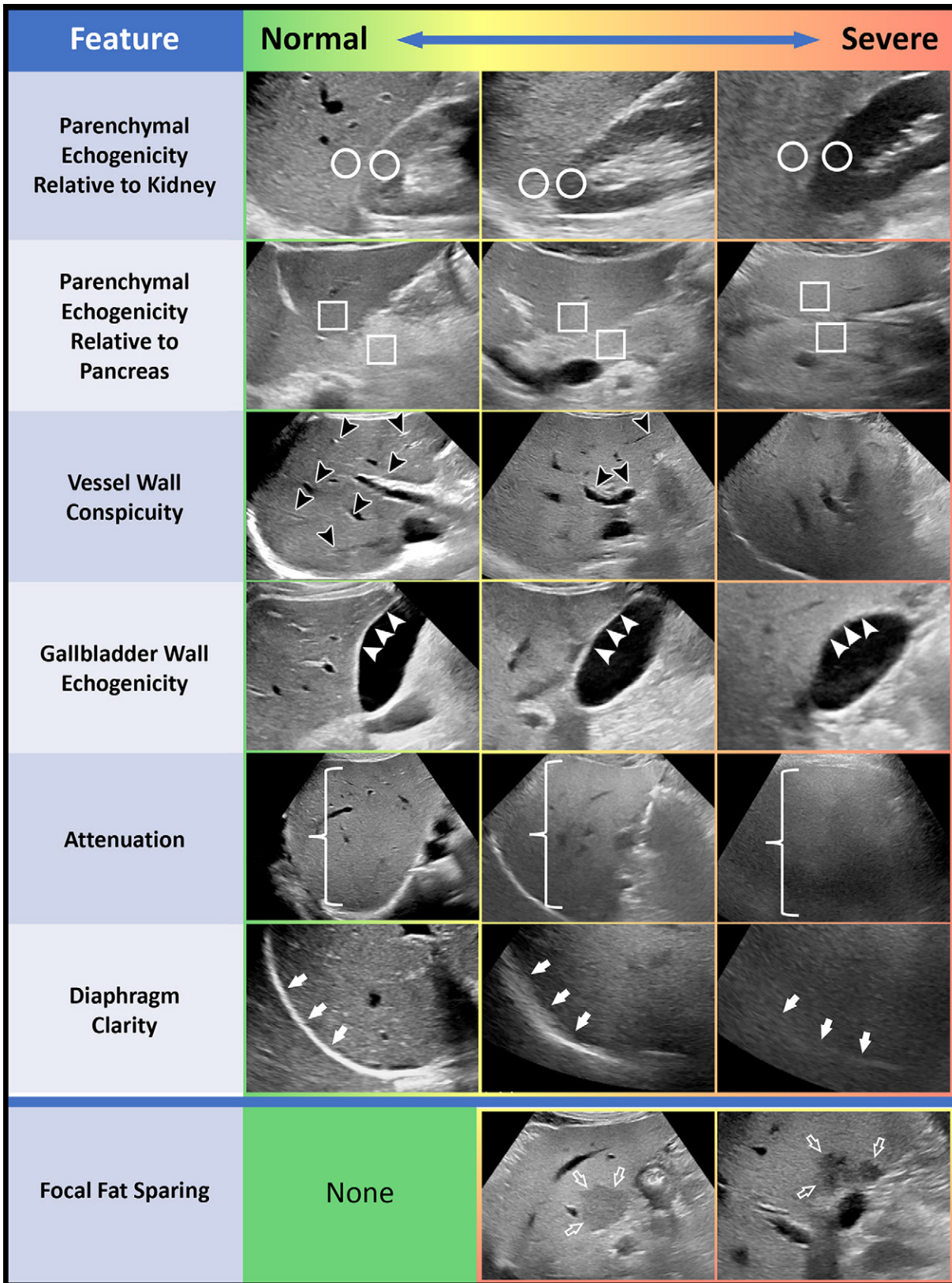


Figure 9. Examples of classic B-mode gray-scale US features of hepatic steatosis, ranging from none (normal) to severe. Liver parenchymal echogenicity relative to the right renal cortex at the same depth (circles) will progressively increase. Parenchymal echogenicity may also increase relative to that of the pancreas (squares). As steatosis increases, the relative echogenicity and conspicuity of vessel walls will decrease (black arrowheads), first affecting the hepatic vein walls, then portal veins. Similarly, the relative echogenicity of the gallbladder wall (white arrowheads) will decrease. Increasing parenchymal attenuation due to steatosis may be perceived as progressive darkening of hepatic parenchyma further from the transducer (bracket), despite time-gain compensation (TGC) adjustments. The clarity and echogenicity of the diaphragm will also diminish as steatosis increases (solid arrows) owing to loss of relative echogenicity, increased attenuation, and poor echo localization due to variations in SoS. Focal fat sparing (open arrows) is not seen in a normal liver and is a specific sign for any degree of steatosis.



**Figure 10.** Hepatorenal index (HRI) in a normal healthy patient. US image shows a representative HRI measurement in a 63-year-old man with less than 6% liver fat fraction at MR-PDFF, a value indicating absence of significant steatosis. Circular ROIs have been placed in the renal cortex and adjacent liver at the same distance from the transducer. The HRI is 1.35, considered a normal value.

and the attenuation coefficient—the loss of acoustic magnitude (in decibels) over a specific depth range (in centimeters) at a specific frequency (in megahertz)—is calculated (Figs 13–20). In biologic tissues, the attenuation coefficient ranges from 0.01 to 4 dB/cm/MHz (27). In the liver, the attenuation coefficient is expected to range from 0.43 to 1.26 dB/cm/MHz (31,45). Both the time-domain method and frequency-domain method have been investigated for attenuation measurements, with modern methods relying on estimating spectral differences or spectral shift (27,31). Historically, after measurement of the attenuation coefficient, a subsequent acquisition on a tissue-mimicking reference phantom using the same system settings and ROI depth was required for calibration (46).

**Advantages.**—The attenuation coefficient is relatively intuitive and straightforward to perform. With increasing bandwidth, sensitivity, stability, and reproducibility of commercial US systems, calibration data from a reference phantom can be programmed into the imaging system, allowing easier clinical implementation without the need for external calibration (46,47).

**Limitations.**—Confounders may include ROI size, depth, near-field reverberation and phase-aberration artifacts from the abdominal wall, fasting status, and liver heterogeneity (31). The attenuation coefficient is not a direct measure of fat content, and other processes such as superimposed liver fibrosis may also influence attenuation.

### Backscatter Coefficient

**Concept.**—The backscatter coefficient refers to measurement of ultrasound echoes attributed to reflection and scattering, data that are the primary determinant of gray-scale brightness in B-mode imaging (27) (Fig 6). Ideally, the backscatter coefficient is a fundamental measure independent of US system characteris-

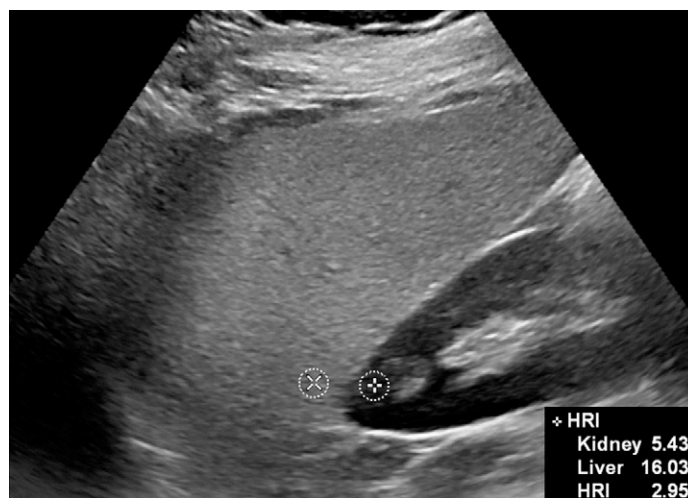


**Figure 11.** Hepatorenal index (HRI) in a 64-year-old woman with 18% fat fraction at MR-PDFF, indicating moderate steatosis. Circular ROIs have been placed in the renal cortex and adjacent liver at the same distance from the transducer. US image shows an HRI of 2.95, considered abnormally elevated.

tics and settings, transducer properties, and attenuation between the ultrasound probe and the selected ROI (48,49). It is usually reported at a single frequency, although spectral information over the transducer bandwidth can be quantitatively analyzed with descriptive modeling (beyond the scope of this review).

**Measurement Method.**—Similar to the attenuation coefficient, the backscatter coefficient is measured within a large liver ROI in units of  $\text{cm}^{-1} \text{sr}^{-1}$ , where  $\text{sr}$  signifies a solid angle in steradians (27). Liver backscatter coefficient at 3 MHz typically ranges from  $0.5 \pm 0.2 \times 10^{-3} \text{ cm}^{-1} \text{sr}^{-1}$  in normal livers to  $6.8 \pm 3.7 \times 10^{-3} \text{ cm}^{-1} \text{sr}^{-1}$  in fatty livers (50). Calculation of the backscatter coefficient requires scanner raw (radiofrequency) data, and compensation for system settings and beam characteristics is needed, which has traditionally required calibration with a reference phantom, similar to the attenuation coefficient.

**Advantages.**—The backscatter coefficient provides a quantitative signature of tissue microstructure. A correlation of 0.80 (Spearman rank correlation,  $P < .0001$ ) was reported between the backscatter coefficient at 2.9–3.1 MHz and MRI-PDFF (range of 5%–35%) (51). In a cohort with MRI-PDFF ranging from 0.7%–41%, a correlation of 0.58 (Pearson correlation,  $P < .001$ ) was documented with the backscatter coefficient at 2.3–3.1 MHz (52).

**Limitations.**—The backscatter coefficient is not directly available on current clinical systems. Accurate measurement of backscatter coefficient requires accurate accounting of system setting and beam characteristics, although scanners with embedded calibrations are emerging for clinical imaging. Similar to the attenuation coefficient, confounders may include ROI size, depth, near-field reverberation and phase-aberration artifacts, fasting status, and liver heterogeneity (53). The backscatter coefficient is not a direct measure of fat content, and other processes such as superimposed liver fibrosis may also influence backscatter.

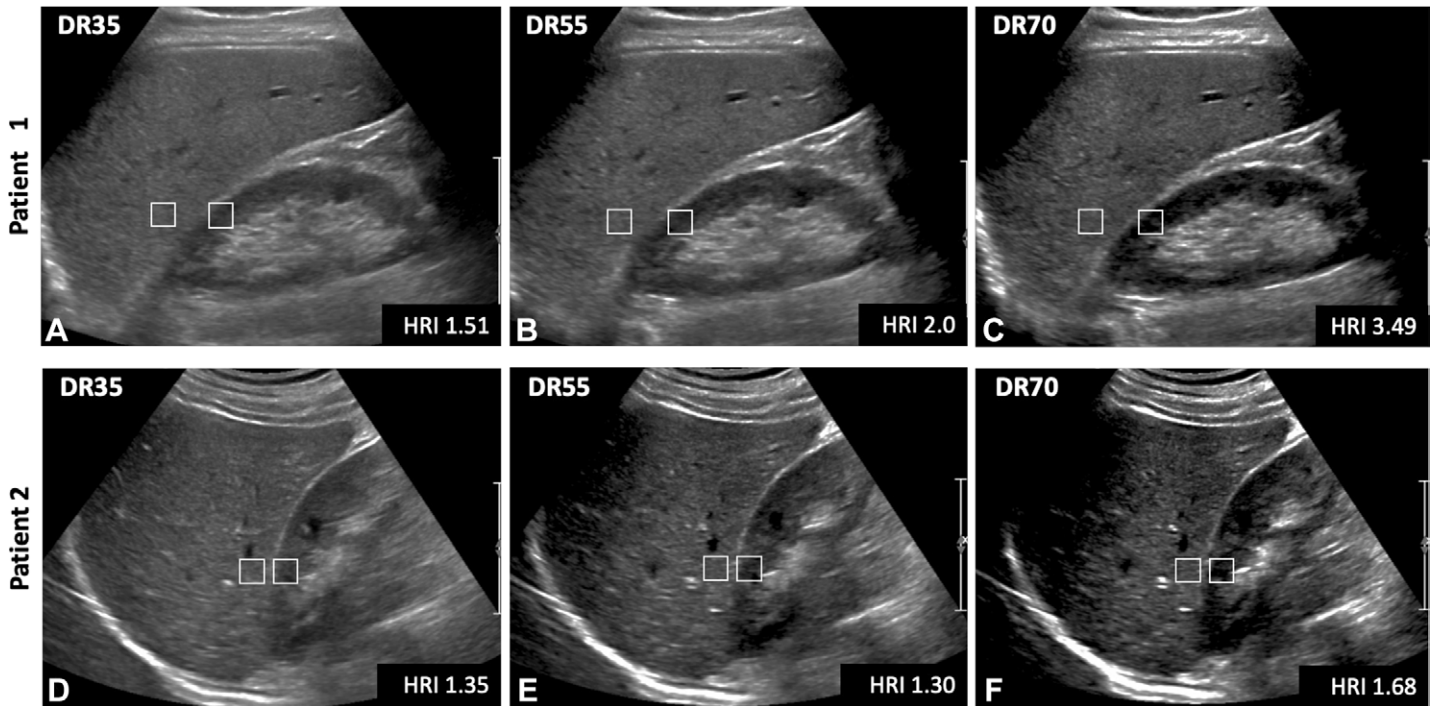


Figure 12. Technique-dependent variation in hepatorenal index (HRI) results. Gray-scale US images of the right kidney and adjacent liver in two patients (patient 1, A–C; patient 2, D–F) show variability in HRI induced by changes to dynamic range (DR) settings (DR35, DR55, and DR70). The HRI for patient 1 yields mild steatosis (with 1.49 used as the cutoff) at DR35 and severe steatosis at DR70. The HRI for patient 2 yields no steatosis at DR35 and mild steatosis at DR70.

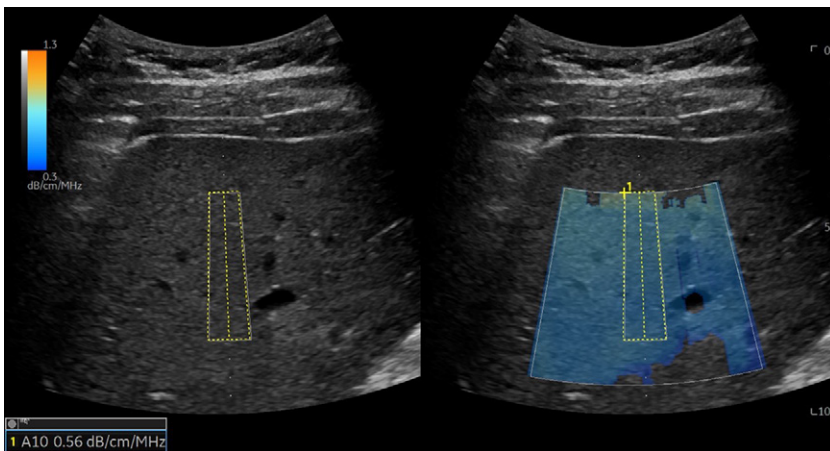


Figure 13. Representative US-derived hepatic attenuation measurement (UGAP; GE Healthcare) in a 41-year-old man without a history of liver disease, significant alcohol use, or metabolic syndrome. Color map superimposed on a background B-mode US image of the liver provides a visual representation of attenuation values from 0.3 to 1.3 dB/cm/MHz. The hepatic attenuation measurement, 0.56 dB/cm/MHz, is derived from the yellow box ROI and is within the lower range of expected liver attenuation values.

**Speed of Sound**

**Concept.**—SoS is the longitudinal compression (acoustic) wave propagation velocity in a medium, which varies depending on material composition—for example, 1450 m/sec in fat and 1550 m/sec in liver (28). Medical US image formation assumes a single constant SoS, typically 1540 m/sec. Tissue SoS deviations cause echo depth localization errors and image quality degradation, often appreciated as reduced lateral resolution and decreased speckle brightness (27) (Fig 5). In the liver, SoS is inversely correlated with steatosis.

**Measurement Method.**—SoS is reported in meters per second. Some manufacturers permit manual selection of SoS used for beam forming, although qualitative image assessment is re-

quired for SoS estimation. Numerous quantitative techniques permit SoS estimation (27,28).

Focusing techniques seek to optimize image lateral resolution and speckle brightness by iteratively varying SoS until image quality is maximized. Similarly, coherence techniques optimize image quality, although at the channel level rather than the image level. Compounding techniques measure the time delay between echoes generated from various pulse transmit angles. Several manufacturers can estimate SoS, either averaged over an image or within an ROI, reported as SoS (eg, 1550 m/sec) or as a deviation from 1540 m/sec (eg, +10) (Figs 19, 20).

**Advantages.**—SoS is intuitive, inversely associated with steatosis level, and frequency independent and has homogeneous

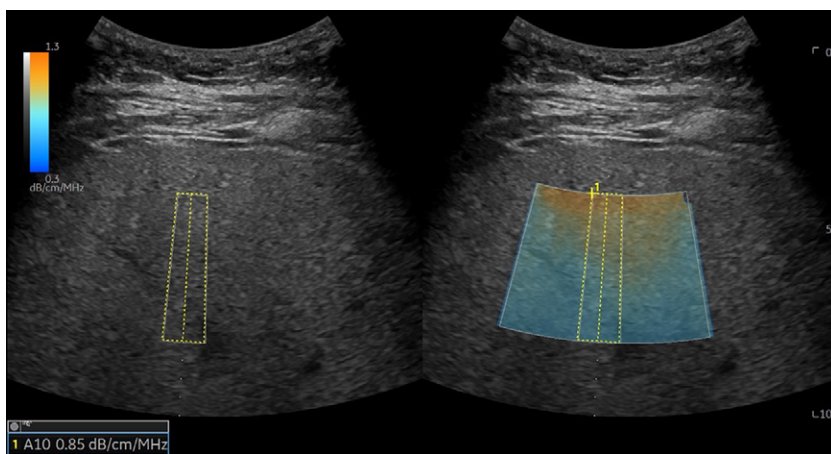


**Figure 14.** Representative US-derived hepatic attenuation measurement (UGAP; GE Healthcare) in a 34-year-old man with 16% fat fraction based on prior MRI-PDFF (not shown), indicating mild steatosis. Color map superimposed on a background B-mode US image of the liver provides a visual representation of attenuation values from 0.3 to 1.3 dB/cm/MHz. The hepatic attenuation measurement, 0.85 dB/cm/MHz, is higher than that of a normal liver imaged with the same device owing to fat deposition.

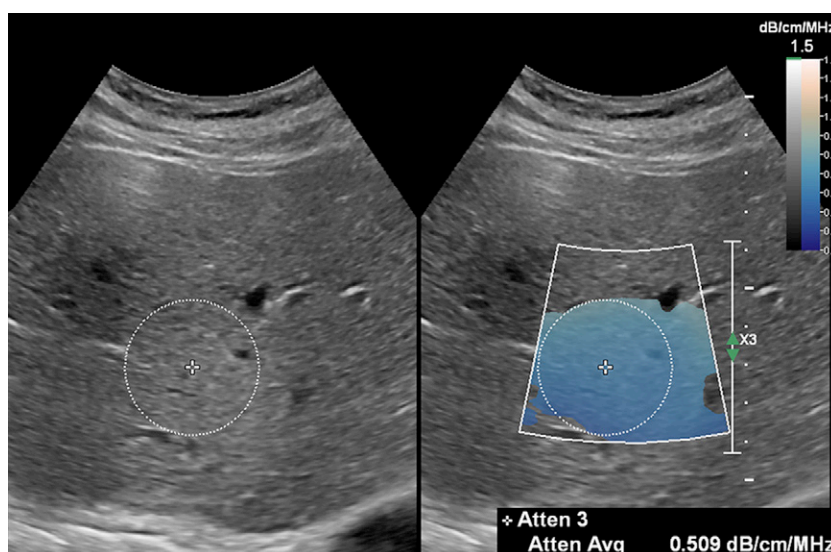


**Figure 15.** Representative US-derived hepatic attenuation measurement (Atten; Philips Healthcare) in a 57-year-old man with less than 6% fat fraction based on prior MRI-PDFF (not shown), indicating no significant steatosis. Color map superimposed on a background B-mode US image of the liver provides a visual representation of attenuation values from 0.0 to 1.5 dB/cm/MHz. The hepatic attenuation measurement, 0.51 dB/cm/MHz, is derived from the circular ROI and is within the lower range of expected liver attenuation values.

reporting methodology. Beyond its role as a biomarker, SoS estimation can also improve image quality.

**Limitations.**—SoS estimation is currently limited to a few manufacturers, and the impacts of transmit frequency and ROI size and depth require further investigation. There is a relatively narrow range of expected SoS in liver (1400–1700 m/sec), requiring high measurement precision and minimized bias (27). As with the attenuation coefficient and backscatter coefficient, confounders may include near-field reverberation artifacts, fasting status, and liver heterogeneity, and motion may introduce measurement error (28). SoS is not a direct measure of fat content, and concomitant liver fibrosis—which increases SoS—confounds hepatic fat estimation. Therefore, techniques such as shear wave elastography (SWE) for fibrosis estimation may be needed.

#### Composite Quantitative Techniques

**Concept.**—Individual quantitative biomarkers may be impacted by confounders, wide ranges in cutoff values, and overlap between steatosis grades (26,27,54). Combination of several quantitative parameters into a composite technique may correct

for sources of variability and improve correlation with liver fat content. One such method—modeling phantom-corrected attenuation and backscatter—has shown promise, now commercially available as US-derived fat fraction (UDFF) (46,52,55).

**Measurement Method.**—UDFF provides a quantitative parameter of hepatic fat within a 3-cm ROI positioned perpendicular to and 1.5–2 cm below the liver capsule in an artifact-free area, avoiding masses and large vessels. The UDFF index is calculated by nonlinear regression of the attenuation coefficient and backscatter coefficient using embedded reference phantom calibrations (55). Results are reported in percent, similar to MRI-PDFF (Figs 21, 22). Unlike the nonlinear correlation of the attenuation coefficient and backscatter coefficient, UDFF shows a linear relationship with PDFF (56).

**Advantages.**—UDFF may be combined with routine liver US with an examination time of less than 5 minutes and has shown good interobserver agreement (56). With histologic steatosis used as a reference, the diagnostic accuracy for detecting the presence of steatosis in greater than 5% of hepatocytes was originally reported as 0.94 (0.85–0.98), comparable with that of MRI-PDFF (55). One recent study reported an

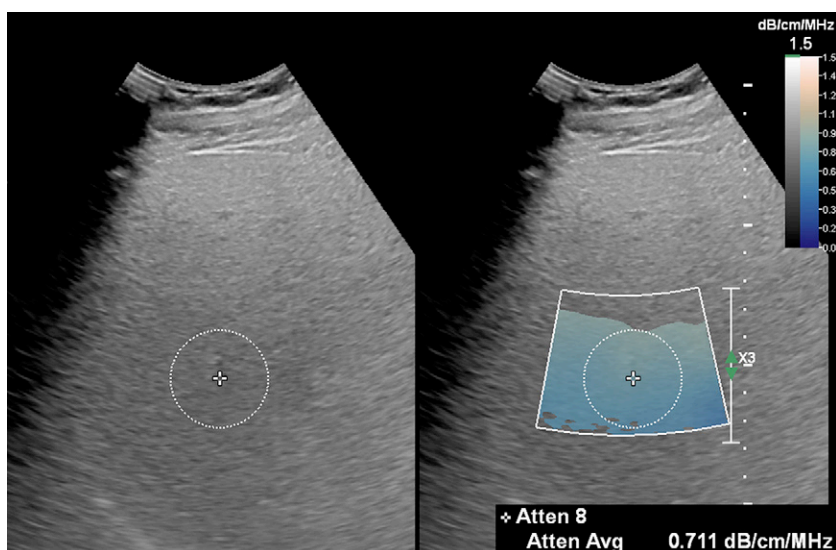


**Figure 16.** Representative US-derived hepatic attenuation measurement (Atten; Philips Healthcare) in a 65-year-old man with 17% fat fraction based on prior MRI-PDFF (not shown), indicating mild to moderate hepatic steatosis. Color map superimposed on a background B-mode US image of the liver provides a visual representation of attenuation values from 0.0 to 1.5 dB/cm/MHz. The hepatic attenuation measurement, 0.71 dB/cm/MHz, is derived from the circular ROI and is higher than that of a normal liver imaged with the same device as a consequence of hepatic steatosis.

AUROC of 0.90 for identification of MRI-PDFF of 5.5% or greater (56). Measurement of UDFP may simultaneously provide shear wave speed measurements of liver stiffness for fibrosis estimation.

**Limitations.**—As UDFP is a propriety technique, intervendor comparisons may be challenging. The large ROI used by UDFP may be limited by a narrow acoustic window and a small right lobe and may be confounded by liver masses and inhomogeneous fat distribution.

## Future US Techniques

### Advanced US Data Analysis

**Concept.**—The standard gray-scale B-mode image is highly processed by filtering, compression, compounding, and various despeckling (smoothing) techniques. Behind these images is a large amount of raw backscatter data that is available for various advanced and future quantitative analyses. These data are often referred to as radiofrequency or in-phase (I) and quadrature (Q) demodulated (I/Q) data, analysis of which has led to innovations in various quantitative techniques in liver disease (27).

**Measurement Method.**—Radiofrequency and I/Q data are collected by the scanner for every image obtained and may be saved in the US device; however, they are generally not exported to the PACS. Once extracted from the scanner, data require significant processing.

**Postprocessing.**—Radiofrequency and I/Q data processing allows analysis of liver steatosis by modeling the intensity occurrence distribution (or histogram) of backscatter speckle with probability density functions (57), the most common including the Rayleigh, homodyned-K, and Nakagami statistical models, and comparing the results with those of normal liver. Parameters used to fit the model histogram can be presented in the form of color parametric images.

Radiofrequency processing may also allow additional analysis of SWE data for various liver disease states. For example, shear wave attenuation (which differs from compression wave attenuation, typically assessed with CAP, or the attenuation coefficient) also increases with liver steatosis grade (58). Differences of the shear wave speed with frequency can be measured as shear wave dispersion (SWD) and also displayed as a parametric image (59).

**Advantages.**—Preclinical studies have shown the value of homodyned-K and Nakagami modeling to assess liver steatosis (60,61). In rat models, homodyned-K imaging improved the grading of superimposed liver inflammation when added to SWE (62). A Nakagami imaging strategy provided AUROCs for grading human steatosis of 0.76 (mild), 0.81 (moderate), and 0.82 (severe) (63). Today, a few US system manufacturers are offering speckle statistics imaging capabilities (64,65) (Fig 23).

SWD appears to correlate with steatosis grade (59). SWD can describe liver viscosity (or damping property) and is also considered sensitive to lobular inflammation in early studies (66,67). SWD is now implemented on some clinical devices (Figs 24, 25).

**Limitations.**—Not all manufacturers allow direct access to the radiofrequency and I/Q data, and some may require a specific research agreement. Analyzing and modeling radiofrequency and I/Q data often require special expertise, and results may not be intuitive. Further studies are needed to assess translatability, reproducibility, and reliability in assessing various liver disease states.

### Artificial Intelligence–based Techniques

**Concept.**—An emerging trend is use of artificial intelligence algorithms to detect or grade the severity of steatosis (52,68,69). The input training dataset may include B-mode or postprocessed radiofrequency acquisition data. The reference standard may be visual assessment of liver fat by radiologists, liver biopsy results, or MRI-PDFF (68,69).

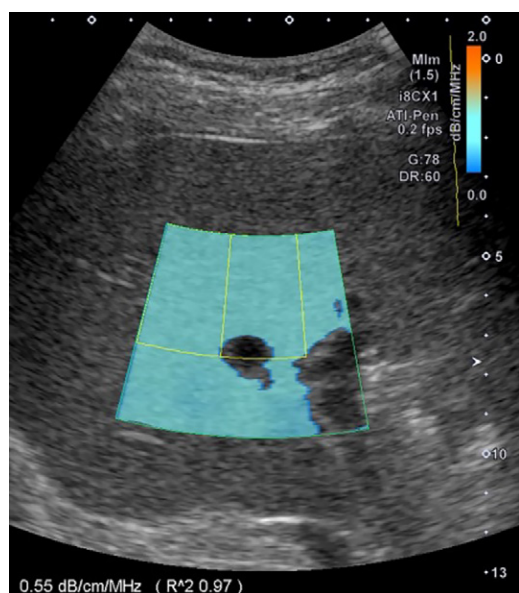


**Figure 17.** Representative US-derived hepatic attenuation measurement (ATI; Canon Medical Systems) in a 41-year-old man without a history of liver disease, significant alcohol use, or metabolic syndrome. Color map superimposed on a background B-mode US image of the liver provides a visual representation of attenuation values from 0.0 to 2.0 dB/cm/MHz. High attenuation is represented by orange or red. Low confidence measurements, such as in the bottom right of the region, are not displayed. The hepatic attenuation measurement, 0.55 dB/cm/MHz, is derived from the inset yellow sector ROI and is within the lower range of expected liver attenuation values. The high  $R^2$  value, 0.97, indicates a high-quality measurement.



**Figure 18.** Representative US-derived hepatic attenuation measurement (ATI; Canon Medical Systems) in a 34-year-old man with 16% fat fraction based on prior MRI-PDFF (not shown), indicating mild hepatic steatosis. Color map superimposed on a background B-mode US image of the liver provides a visual representation of attenuation values from 0.0 to 2.0 dB/cm/MHz. The hepatic attenuation measurement, 0.85 dB/cm/MHz, is higher than that of a normal liver imaged with the same device owing to hepatic steatosis. The  $R^2$  value, 0.99, indicates that this is a high-quality measurement.

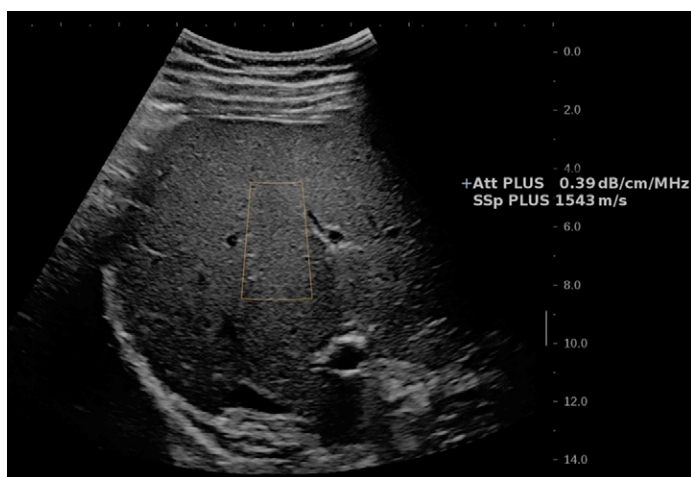


**Figure 19.** Representative US-derived hepatic attenuation and SoS measurements (Att PLUS; SuperSonic Imagine) in a 41-year-old man without a history of liver disease, significant alcohol use, or metabolic syndrome. The hepatic attenuation measurement, 0.39 dB/cm/MHz, and SoS measurement, 1543 m/sec, are derived from the box-shaped ROI superimposed on a background B-mode US image of the liver and are considered normal values.

**Measurement method.**—Assessment of steatosis severity has been proposed on single representative reproducible images, either on the entire US image or after segmentation. Classification of liver steatosis severity with convolutional neural

networks has been approached as a two-way classification (ie, normal vs fatty liver) (70), multiway classification (ie, steatosis grades 0, 1, 2, and 3) (71), or regression problem (ie, prediction of the liver fat fraction as a percentage) (69).

**Advantages.**—Promising results have been reported for grading the severity of liver steatosis (69,71). Once models are trained, the predictions can be run in real time, displaying results as the images are acquired.

**Limitations.**—Numerous technical sources of variability may affect US images: US scanner manufacturers, models, probes, image settings, and image views. Therefore, robustness and generalization of models must be assessed in different populations and with different equipment before clinical use.

### Comprehensive Assessment of Liver Disease

Hepatic steatosis is one of many conditions that may affect the liver. Multiparametric imaging has been considered necessary for comprehensive assessment of liver disease, which may include steatosis, inflammation, hepatocyte ballooning, and fibrosis (27,72–75). A combination of US parameters including the hepatorenal index, attenuation coefficient, backscatter coefficient, SoS, SWE, SWD, and Nakagami and homodyned-K parameters could all be used in combination in multivariate linear models, logistic regressions, or machine learning strategies to correct for confounders and improve

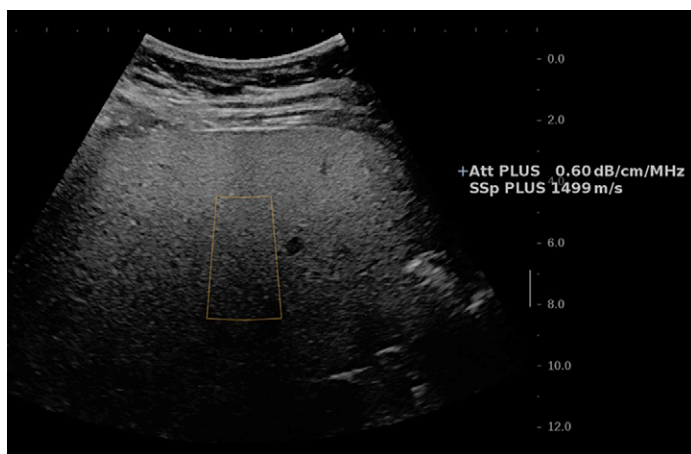


**Figure 20.** Representative US-derived hepatic attenuation and SoS measurements (Att PLUS; SuperSonic Imagine) in a 34-year-old man with 16% fat fraction based on prior MRI-PDFF (not shown), indicating mild steatosis. The hepatic attenuation measurement, 0.60 dB/cm/MHz (higher than that of normal liver imaged with the same device), and hepatic SoS measurement, 1499 m/sec (lower than that of normal liver), are derived from the box-shaped ROI superimposed on a background B-mode US image of the liver. These changes are an expected consequence of hepatic steatosis.

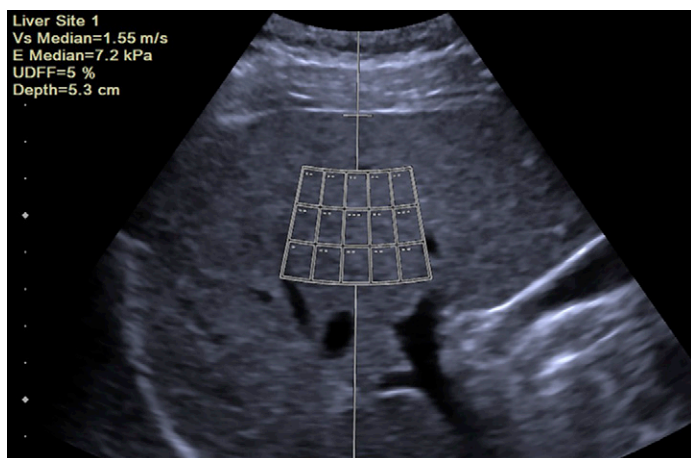


**Figure 21.** Representative steatosis measurement (UDFF; Siemens Healthineers) in a 41-year-old man without a history of liver disease, significant alcohol use, or metabolic syndrome. UDFF is calculated from measurements from a sector region, which is superimposed on a background B-mode US image of the liver. Additionally, shear wave velocity is measured in 15 ROIs within the sector. The UDFF value, a composite metric based on attenuation and backscatter and normalized to MR-PDFF, is 5%.

the diagnostic performance of US for precise characterization of liver disease. Advancement of these techniques will certainly benefit from the technical standardization processes led by the RSNA's Quantitative Imaging Biomarkers Alliance (QIBA).

### Conclusion

Given the increased prevalence, awareness, and clinical impact of hepatic steatosis, US is well positioned to function as an impactful screening and surveillance tool. There are many new and emerging quantitative techniques that hold great promise beyond the routinely used qualitative assessment of the gray-scale features of steatosis. Future efforts are likely to focus on composite and multiparametric tech-

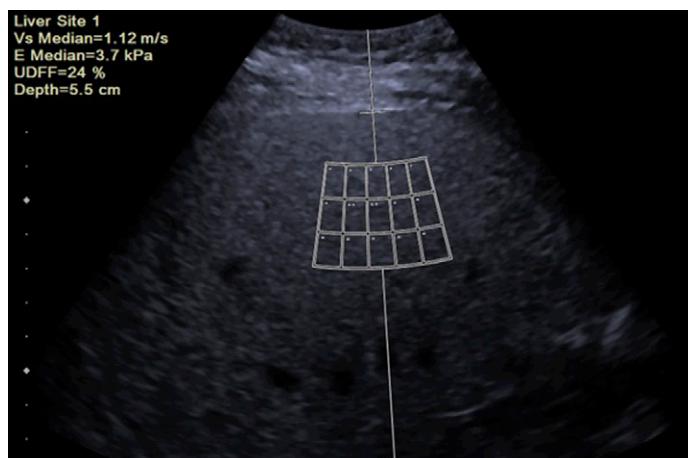


**Figure 22.** Representative UDFF measurement (UDFF; Siemens Healthineers) in a 34-year-old man with 16% fat fraction on the basis of prior MRI-PDFF (not shown), indicating mild steatosis. UDFF is calculated from measurements from a sector region, which is superimposed on a background B-mode US image of the liver. Additionally, shear wave velocity is measured in 15 ROIs within the sector. The UDFF value—a composite metric based on attenuation and backscatter and normalized to MR-PDFF—is 24%, higher than that of normal liver imaged with the same device owing to hepatic steatosis.

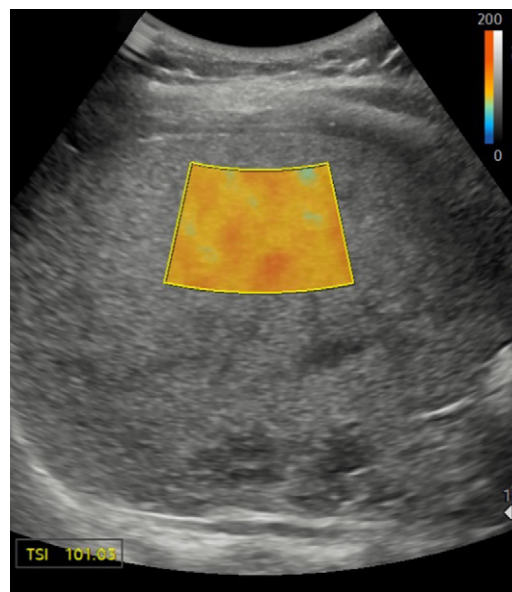


**Figure 23.** Representative tissue scatter distribution imaging (TSI) measurement (Samsung Medison) in a 40-year-old woman with incidental hepatic steatosis. Color map superimposed on a background B-mode US image of the liver shows the TSI value. Studies regarding correlation of TSI output (number and color map) with steatosis are ongoing. (Courtesy of Stephanie Wilson, MD, University of Calgary, Calgary, Alberta, Canada.)

niques, with or without advanced backscatter data analytics and artificial intelligence.

**Author affiliations.**—From the Department of Radiology (D.T.F.) and Department of Internal Medicine, Division of Digestive and Liver Diseases (A.M.), UT Southwestern Medical Center, 5323 Harry Hines Blvd, E6-230-BF, Dallas, TX 75390-9316; Department of Radiology, Massachusetts General Hospital and Harvard Medical School, Boston, Mass (T.T.P.); Department of Radiology, University of Alabama at Birmingham, Birmingham, Ala (M.L.R.);

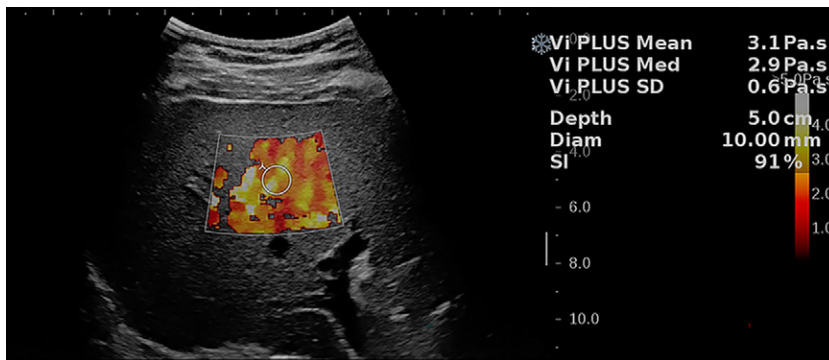


Figure 24. Representative US-derived hepatic viscosity measurement (Vi PLUS; SuperSonic Imagine) in a 41-year-old man without a history of liver disease, significant alcohol use, or metabolic syndrome. Color map superimposed on a background B-mode US image of the liver provides a visual representation of viscosity values. The yellow and white pixels indicate higher viscosity. The hepatic viscosity measurement, 3.1 Pa · sec, is derived from the inlayed circular ROI.

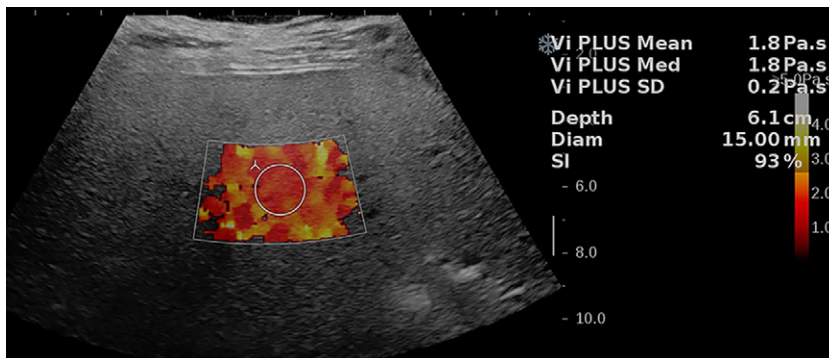


Figure 25. Representative US-derived hepatic viscosity measurement (Vi PLUS; SuperSonic Imagine) in a 34-year-old man with 16% fat fraction on the basis of prior MRI-PDFF (not shown), indicating mild steatosis. Color map superimposed on a background B-mode US image of the liver provides a visual representation of viscosity values. The red and orange pixels indicate lower viscosity. The hepatic viscosity measurement, 1.8 Pa · sec, is derived from the inlayed circular ROI, lower than expected owing to hepatic steatosis.

Departments of Radiology and Biomedical Engineering, Laboratory of Biomechanics and Medical Ultrasonics, University of Montréal Hospital Research Center, Montréal, Quebec, Canada (G.C.); Department of Medical Physics, University of Wisconsin, Madison, Wis (T.J.H.); Department of Radiology, University of Kansas Medical Center, Kansas City, Kan (A.C.); Department of Diagnostic and Interventional Radiology, University Hospital Homburg/Saar, Homburg, Germany (R.K.); and Department of Radiology, Centre Hospitalier de l'Université de Montréal (CHUM) and Université de Montréal, Montréal, Quebec, Canada (A.T.). Presented as an education exhibit at the 2021 RSNA Annual Meeting. Received July 25, 2022; revision requested September 27 and received October 31; accepted November 07. **Address correspondence** to D.T.F. (email: [David.Fetzer@UTSouthwestern.edu](mailto:David.Fetzer@UTSouthwestern.edu)).

**Acknowledgments.**—We would like to acknowledge Stephanie Wilson, MD, University of Calgary, and David Hunt, RDMS, RT(S), RVT, Massachusetts General Hospital, for assisting with image and case collection for the manuscript.

**Funding.**—T.T.P. supported by a 2020 ARRS Scholar Award from the American Roentgen Ray Society. A.T. supported by a senior clinical research scholarship from Fonds de Recherche du Québec en Santé (FRQ-S) and Fondation de l'Association des Radiologistes du Québec (FRQS-ARQ 298509).

**Disclosures of conflicts of interest.**—D.T.F. Research agreements with GE Healthcare, Philips Healthcare, and Siemens Healthineers; advisory board for GE Healthcare and Philips Healthcare. T.T.P. Grants [unrelated] from General Electric, Massachusetts Institute of Technology, Massachusetts General Hospital, and National Institutes of Health; salary support [unrelated] from GE Healthcare, National Institutes of Health, and Department of Defense; royalty from UpToDate; honoraria for lecture from Massachusetts Society for Radiologic Technologists; patent 631020.00099: Systems and Methods for Portable Ultrasound Guided Cannulation. M.L.R. Research agreement with Philips Medical. G.C. Research agreement with Siemens Healthineers, loan of a US system for research from Siemens Healthineers. T.J.H. Payment from RSNA in support of leadership service to the Quantitative Imaging Biomarkers Alliance; grants from Pfizer and Siemens Healthineers, Ultrasound Division; equipment loans and technical support from Siemens Healthineers, Ultrasound Division; operates fee-for-service custom US phantom development, production, and calibration service for industry and academic laboratories. A.C. Research agreement with Siemens Healthineers. A.T. Operating grant from Canadian Institutes of Health Research, equipment loan (US scanner) from Siemens Healthineers for research study. All other authors, the editor, and the reviewers have disclosed no relevant relationships.

## References

- Chalasan N, Younossi Z, Lavine JE, et al. The diagnosis and management of nonalcoholic fatty liver disease: practice guidance from the American Association for the Study of Liver Diseases. *Hepatology* 2018;67(1):328–357.
- Schwabe RF, Tabas I, Pajvani UB. Mechanisms of Fibrosis Development in Nonalcoholic Steatohepatitis. *Gastroenterology* 2020;158(7):1913–1928.
- Younossi ZM, Stepanova M, Afendy M, et al. Changes in the prevalence of the most common causes of chronic liver diseases in the United States from 1988 to 2008. *Clin Gastroenterol Hepatol* 2011;9(6):524–530.e1; quiz e60.
- Younossi ZM, Koenig AB, Abdelatif D, Fazel Y, Henry L, Wymer M. Global epidemiology of nonalcoholic fatty liver disease: meta-analytic assessment of prevalence, incidence, and outcomes. *Hepatology* 2016;64(1):73–84.
- Estes C, Anstee QM, Arias-Loste MT, et al. Modeling NAFLD disease burden in China, France, Germany, Italy, Japan, Spain, United Kingdom, and United States for the period 2016–2030. *J Hepatol* 2018;69(4):896–904.
- Younossi Z, Henry L. Contribution of Alcoholic and Nonalcoholic Fatty Liver Disease to the Burden of Liver-related Morbidity and Mortality. *Gastroenterology* 2016;150(8):1778–1785.
- Adams LA, Anstee QM, Tilg H, Targher G. Non-alcoholic fatty liver disease and its relationship with cardiovascular disease and other extrahepatic diseases. *Gut* 2017;66(6):1138–1153.
- Younossi ZM, Otgonsuren M, Henry L, et al. Association of nonalcoholic fatty liver disease (NAFLD) with hepatocellular carcinoma (HCC) in the United States from 2004 to 2009. *Hepatology* 2015;62(6):1723–1730.
- Younossi Z, Stepanova M, Ong JP, et al; Global Nonalcoholic Steatohepatitis Council. Nonalcoholic Steatohepatitis Is the Fastest Growing Cause of Hepatocellular Carcinoma in Liver Transplant Candidates. *Clin Gastroenterol Hepatol* 2019;17(4):748–755.e3.
- Allen AM, Van Houten HK, Sangaralingham LR, Talwalkar JA, McCoy RG. Healthcare Cost and Utilization in Nonalcoholic Fatty Liver Disease: Real-World Data from a Large U.S. Claims Database. *Hepatology* 2018;68(6):2230–2238.
- Bedossa P, Dargère D, Paradis V. Sampling variability of liver fibrosis in chronic hepatitis C. *Hepatology* 2003;38(6):1449–1457.
- Fedchuk L, Nascimbeni F, Pais R, Charlotte F, Housset C, Ratziu V; LIDO Study Group. Performance and limitations of steatosis biomarkers in patients with nonalcoholic fatty liver disease. *Aliment Pharmacol Ther* 2014;40(10):1209–1222.
- Zhou Y, Orešič M, Leivonen M, et al. Noninvasive Detection of Nonalcoholic Steatohepatitis Using Clinical Markers and Circulating Levels of Lipids and Metabolites. *Clin Gastroenterol Hepatol* 2016;14(10):1463–1472.e6.

14. Sasso M, Beaugrand M, de Ledinghen V, et al. Controlled attenuation parameter (CAP): a novel VCTE™ guided ultrasonic attenuation measurement for the evaluation of hepatic steatosis—preliminary study and validation in a cohort of patients with chronic liver disease from various causes. *Ultrasound Med Biol* 2010;36(11):1825–1835.
15. Ferraioli G, Tinelli C, Lissandrini R, et al. Controlled attenuation parameter for evaluating liver steatosis in chronic viral hepatitis. *World J Gastroenterol* 2014;20(21):6626–6631.
16. Eddowes PJ, Sasso M, Allison M, et al. Accuracy of FibroScan Controlled Attenuation Parameter and Liver Stiffness Measurement in Assessing Steatosis and Fibrosis in Patients with Nonalcoholic Fatty Liver Disease. *Gastroenterology* 2019;156(6):1717–1730.
17. Petroff D, Blank V, Newsome PN, et al. Assessment of hepatic steatosis by controlled attenuation parameter using the M and XL probes: an individual patient data meta-analysis. *Lancet Gastroenterol Hepatol* 2021;6(3):185–198.
18. Starekova J, Reeder SB. Liver fat quantification: where do we stand? *Abdom Radiol (NY)* 2020;45(11):3386–3399.
19. Starekova J, Hernando D, Pickhardt PJ, Reeder SB. Quantification of Liver Fat Content with CT and MRI: State of the Art. *Radiology* 2021;301(2):250–262.
20. Reeder SB, Cruite I, Hamilton G, Sirlin CB. Quantitative Assessment of Liver Fat with Magnetic Resonance Imaging and Spectroscopy. *J Magn Reson Imaging* 2011;34(4):729–749.
21. Pickhardt PJ, Graffy PM, Reeder SB, Hernando D, Li K. Quantification of Liver Fat Content with Unenhanced MDCT: Phantom and Clinical Correlation with MRI Proton Density Fat Fraction. *AJR Am J Roentgenol* 2018;211(3):W151–W157.
22. Ma X, Holalkere NS, Kambadakone R A, Mino-Kenudson M, Hahn PF, Sahani DV. Imaging-based quantification of hepatic fat: methods and clinical applications. *RadioGraphics* 2009;29(5):1253–1277.
23. Pickhardt PJ, Graffy PM, Perez AA, Lubner MG, Elton DC, Summers RM. Opportunistic Screening at Abdominal CT: Use of Automated Body Composition Biomarkers for Added Cardiometabolic Value. *RadioGraphics* 2021;41(2):524–542.
24. Tang A, Desai A, Hamilton G, et al. Accuracy of MR imaging—estimated proton density fat fraction for classification of dichotomized histologic steatosis grades in nonalcoholic fatty liver disease. *Radiology* 2015;274(2):416–425.
25. Yokoo T, Serai SD, Pirasteh A, et al; RSNA-QIBA PDFF Biomarker Committee. Linearity, Bias, and Precision of Hepatic Proton Density Fat Fraction Measurements by Using MR Imaging: a Meta-analysis. *Radiology* 2018;286(2):486–498.
26. Ozturk A, Grajo JR, Gee MS, et al. Quantitative Hepatic Fat Quantification in Non-alcoholic Fatty Liver Disease Using Ultrasound-based Techniques: a Review of Literature and Their Diagnostic Performance. *Ultrasound Med Biol* 2018;44(12):2461–2475.
27. Cloutier G, Destrempes F, Yu F, Tang A. Quantitative ultrasound imaging of soft biological tissues: a primer for radiologists and medical physicists. *Insights Imaging* 2021;12(1):127(121)-(120).
28. Imbault M, Faccineto A, Osmanski BF, et al. Robust sound speed estimation for ultrasound-based hepatic steatosis assessment. *Phys Med Biol* 2017;62(9):3582–3598.
29. Insana MF, Hall TJ. Characterising the microstructure of random media using ultrasound. *Phys Med Biol* 1990;35(10):1373–1386.
30. Wagner RF, Smith SW, Sandrik JM, Lopez H. Statistics of Speckle in Ultrasound B-Scans. *IEEE Trans Sonics Ultrason* 1983;30(3):156–163.
31. Ferraioli G, Kumar V, Ozturk A, Nam K, de Korte CL, Barr RG. US Attenuation for Liver Fat Quantification: an AIUM-RSNA QIBA Pulse-Echo Quantitative Ultrasound Initiative. *Radiology* 2022;302(3):495–506.
32. Venkatesh SK, Henneidge T, Johnson GB, Hough DM, Fletcher JG. Imaging patterns and focal lesions in fatty liver: a pictorial review. *Abdom Radiol (NY)* 2017;42(5):1374–1392.
33. Strauss S, Gavish E, Gottlieb P, Katsnelson L. Interobserver and intraobserver variability in the sonographic assessment of fatty liver. *AJR Am J Roentgenol* 2007;189(6):W320–W323.
34. Joseph AE, Saverymuttu SH. Ultrasound in the assessment of diffuse parenchymal liver disease. *Clin Radiol* 1991;44(4):219–221.
35. Nelson SM, Hoskins JD, Lisanti C, Chaudhuri J. Ultrasound Fatty Liver Indicator: a Simple Tool for Differentiating Steatosis from Nonalcoholic Steatohepatitis—Validity in the Average Obese Population. *J Ultrasound Med* 2020;39(4):749–759.
36. Hirooka M, Koizumi Y, Sunago K, et al. Efficacy of B-mode ultrasound-based attenuation for the diagnosis of hepatic steatosis: a systematic review/meta-analysis. *J Med Ultrason* (2001) 2022;49(2):199–210.
37. Hernaez R, Lazo M, Bonekamp S, et al. Diagnostic accuracy and reliability of ultrasonography for the detection of fatty liver: a meta-analysis. *Hepatology* 2011;54(3):1082–1090.
38. Perez NE, Siddiqui FA, Mutchnick MG, et al. Ultrasound diagnosis of fatty liver in patients with chronic liver disease: a retrospective observational study. *J Clin Gastroenterol* 2007;41(6):624–629.
39. Hong CW, Marsh A, Wolfson T, et al. Reader agreement and accuracy of ultrasound features for hepatic steatosis. *Abdom Radiol (NY)* 2019;44(1):54–64.
40. Dasarathy S, Dasarathy J, Khyami A, Joseph R, Lopez R, McCullough AJ. Validity of real time ultrasound in the diagnosis of hepatic steatosis: a prospective study. *J Hepatol* 2009;51(6):1061–1067.
41. Chauhan A, Sultan LR, Furth EE, Jones LP, Khungar V, Sehgal CM. Diagnostic accuracy of hepatorenal index in the detection and grading of hepatic steatosis. *J Clin Ultrasound* 2016;44(9):580–586.
42. Webb M, Yeshua H, Zelber-Sagi S, et al. Diagnostic value of a computerized hepatorenal index for sonographic quantification of liver steatosis. *AJR Am J Roentgenol* 2009;192(4):909–914.
43. Mancini M, Prinster A, Annuzzi G, et al. Sonographic hepatic-renal ratio as indicator of hepatic steatosis: comparison with (1)H magnetic resonance spectroscopy. *Metabolism* 2009;58(12):1724–1730.
44. Marshall RH, Eissa M, Bluth EI, Gulotta PM, Davis NK. Hepatorenal index as an accurate, simple, and effective tool in screening for steatosis. *AJR Am J Roentgenol* 2012;199(5):997–1002.
45. Paige JS, Bernstein GS, Heba E, et al. A Pilot Comparative Study of Quantitative Ultrasound, Conventional Ultrasound, and MRI for Predicting Histology-determined Steatosis Grade in Adult Nonalcoholic Fatty Liver Disease. *AJR Am J Roentgenol* 2017;208(5):W168–W177.
46. Yao LX, Zagzebski JA, Madsen EL. Backscatter coefficient measurements using a reference phantom to extract depth-dependent instrumentation factors. *Ultrason Imaging* 1990;12(1):58–70.
47. Guerrero QW, Fan L, Brunke S, Milkowski A, Rosado-Mendez IM, Hall TJ. Power Spectrum Consistency among Systems and Transducers. *Ultrasound Med Biol* 2018;44(11):2358–2370.
48. Ghoshal G, Mamou J, Oelze ML. State of the Art Methods for Estimating Backscatter Coefficients. In: Mamou J, Oelze ML, eds. *Quantitative Ultrasound in Soft Tissues*. Dordrecht, the Netherlands: Springer, 2013; 3–19.
49. Oelze ML, Mamou J. Review of Quantitative Ultrasound: Envelope Statistics and Backscatter Coefficient Imaging and Contributions to Diagnostic Ultrasound. *IEEE Trans Ultrason Ferroelectr Freq Control* 2016;63(2):336–351.
50. Lu ZF, Zagzebski JA, Lee FT. Ultrasound backscatter and attenuation in human liver with diffuse disease. *Ultrasound Med Biol* 1999;25(7):1047–1054.
51. Lin SC, Heba E, Wolfson T, et al. Noninvasive Diagnosis of Nonalcoholic Fatty Liver Disease and Quantification of Liver Fat Using a New Quantitative Ultrasound Technique. *Clin Gastroenterol Hepatol* 2015;13(7):1337–1345.e6.
52. Han A, Zhang YN, Boehringer AS, et al. Assessment of Hepatic Steatosis in Nonalcoholic Fatty Liver Disease by Using Quantitative US. *Radiology* 2020;295(1):106–113.
53. Nam K, Rosado-Mendez IM, Wirtzfeld LA, et al. Comparison of ultrasound attenuation and backscatter estimates in layered tissue-mimicking phantoms among three clinical scanners. *Ultrason Imaging* 2012;34(4):209–221.
54. Ferraioli G, Berzigotti A, Barr RG, et al. Quantification of Liver Fat Content with Ultrasound: a WFUMB Position Paper. *Ultrasound Med Biol* 2021;47(10):2803–2820.
55. Labyed Y, Milkowski A. Novel Method for Ultrasound-derived Fat Fraction Using an Integrated Phantom. *J Ultrasound Med* 2020;39(12):2427–2438.
56. Dillman JR, Thapaliya S, Tkach JA, Trout AT. Quantification of Hepatic Steatosis by Ultrasound: Prospective Comparison with MRI Proton Density Fat Fraction as Reference Standard. *AJR Am J Roentgenol* 2022;219(5):784–791.
57. Destrempes F, Cloutier G. Review of Envelope Statistics Models for Quantitative Ultrasound Imaging and Tissue Characterization. In: Mamou J, Oelze ML, eds. *Quantitative Ultrasound in Soft Tissues*. Dordrecht, the Netherlands: Springer, 2013; 219–274.
58. Sharma AK, Reis J, Oppenheimer DC, et al. Attenuation of Shear Waves in Normal and Steatotic Livers. *Ultrasound Med Biol* 2019;45(4):895–901.
59. Ormachea J, Parker KJ. Comprehensive Viscoelastic Characterization of Tissues and the Inter-relationship of Shear Wave (Group and Phase) Velocity, Attenuation and Dispersion. *Ultrasound Med Biol* 2020;46(12):3448–3459.
60. Zhou Z, Fang J, Cristea A, et al. Value of homodyned K distribution in ultrasound parametric imaging of hepatic steatosis: an animal study. *Ultrasonics* 2020;101:106001.
61. Ho MC, Lee YH, Jeng YM, Chen CN, Chang KJ, Tsui PH. Relationship between ultrasound backscattered statistics and the concentration of fatty droplets in livers: an animal study. *PLoS One* 2013;8(5):e63543.
62. Tang A, Destrempes F, Kazemirad S, Garcia-Duitama J, Nguyen BN, Cloutier G. Quantitative ultrasound and machine learning for assessment of steatohepatitis in a rat model. *Eur Radiol* 2019;29(5):2175–2184.
63. Fang F, Fang J, Li Q, et al. Ultrasound Assessment of Hepatic Steatosis by Using the Double Nakagami Distribution: a Feasibility Study. *Diagnostics (Basel)* 2020;10(8):557.

64. Jeon SK, Joo I, Kim SY, et al. Quantitative ultrasound radiofrequency data analysis for the assessment of hepatic steatosis using the controlled attenuation parameter as a reference standard. *Ultrasonography* 2021;40(1):136–146.
65. Bae JS, Lee DH, Lee JY, et al. Quantitative Assessment of Fatty Liver using Ultrasound with Normalized Local Variance Technique. *Ultraschall Med* 2020;42(6):599–606.
66. de Araujo Neto JM. Shear-Wave Dispersion Slope: Do We Have the Tool for Detecting Necroinflammation? *Radiology* 2020;294(2):483–484.
67. Sugimoto K, Moriyasu F, Oshiro H, et al. Clinical utilization of shear wave dispersion imaging in diffuse liver disease. *Ultrasonography* 2020;39(1):3–10.
68. Cao W, An X, Cong L, Lyu C, Zhou Q, Guo R. Application of Deep Learning in Quantitative Analysis of 2-dimensional Ultrasound Imaging of Nonalcoholic Fatty Liver Disease. *J Ultrasound Med* 2020;39(1):51–59.
69. Byra M, Han A, Boehringer AS, et al. Liver Fat Assessment in Multiview Sonography Using Transfer Learning with Convolutional Neural Networks. *J Ultrasound Med* 2022;41(1):175–184.
70. Reddy DS, Bharath R, Rajalakshmi P. A Novel Computer-aided Diagnosis Framework Using Deep Learning for Classification of Fatty Liver Disease in Ultrasound Imaging. 2018 IEEE 20th International Conference on e-Health Networking, Applications and Services (Healthcom) 2018:1–5. <https://ieeexplore.ieee.org/document/8531118>.
71. Rhyou SY, Yoo JC. Cascaded Deep Learning Neural Network for Automated Liver Steatosis Diagnosis Using Ultrasound Images. *Sensors (Basel)* 2021;21(16):5304.
72. Destremes F, Gesnik M, Chayer B, et al. Quantitative ultrasound, elastography, and machine learning for assessment of steatosis, inflammation, and fibrosis in chronic liver disease. *PLoS One* 2022;17(1):e0262291.
73. Sugimoto K, Moriyasu F, Oshiro H, et al. The Role of Multiparametric US of the Liver for the Evaluation of Nonalcoholic Steatohepatitis. *Radiology* 2020;296(3):532–540.
74. Pirmoazen AM, Khurana A, Loening AM, et al. Diagnostic Performance of 9 Quantitative Ultrasound Parameters for Detection and Classification of Hepatic Steatosis in Nonalcoholic Fatty Liver Disease. *Invest Radiol* 2022;57(1):23–32.
75. Sugimoto K, Lee DH, Lee JY, et al. Multiparametric US for Identifying Patients with High-Risk NASH: a Derivation and Validation Study. *Radiology* 2021;301(3):625–634.